Title
NUCLEON-NUCLEON POLARIZATION BETWEEN 300 AND TOO MeV

Authors
Cheng, David
Macdonald, Burns
Helland, Jerome A.
et al.

Publication Date
1966-11-15

UCRL-11926 Rev.

University of California

Ernest O. Lawrence Radiation Laboratory

NUCLEON-NUCLEON POLARIZATION BETWEEN 300 AND 700 MeV

Berkeley, California

DISCLAIMER

Submitted to The Physical Review

UCRL-11926 Rev.
Preprint

UNIVERSITY OF CALIFORNIA

Lawrence Radiation Laboratory
Berkeley, California

AEC Contract No. W-7405-eng-48

NUCLEON-NUCLEON POLARIZATION BETWEEN 300 AND 700 MeV

David Cheng, Burns Macdonald, Jerome A. Helland,
and Philip M. Ogden

November 15, 1966

NUCLEON-NUCLEON POLARIZATION BETWEEN 300 AND 700 MeV*

David Cheng, Burns Macdonald†
Lawrence Radiation Laboratory
University of California, Berkeley, California

Jerome A. Helland
University of California, Los Angeles, California

Philip M. Ogden
Seattle Pacific College, Seattle, Washington

November 15, 1966

ABSTRACT

The polarization parameter, $P(\theta^*)$, for pn and pp scattering has been measured at the Berkeley 184-in. cyclotron at beam energies of 310, 400, 500, 600, and 700 MeV. This parameter was measured with a polarized proton beam, which was polarized by scattering at ±6 deg on carbon, then rescattered on an unpolarized nucleon target--a liquid-deuterium target for the pn system; both a liquid hydrogen and a liquid deuterium target for the pp system. Both of the outgoing nucleons from the elastic scatter were detected by an array of 27 scintillation counters in multi-channel coincidences.

In the pp system, $P(\theta^*)$ can be approximated by $A \sin\theta^* \cos\theta^*$, where A varies from 0.85 at 310 MeV to 1.1 at 700 MeV. In the pn system, P_{max} in the forward direction varies from 0.42 at 310 MeV to 0.34 at 700 MeV, and P_{min} in the backward direction varies from -0.25 at 310 MeV to -0.4 at 700 MeV. The shape of the NN polarization curves is nearly independent of energy in this range.

I. INTRODUCTION

Nucleon-nucleon (NN) scattering amplitudes are determined experimentally by scattering experiments in the NN system involving polarizations. In the pp system, there are five (Wolfenstein[1]) amplitudes which are complex functions of energies and c.m. angles ($0 \leqslant \theta^* \leqslant \pi/2$). (See Appendix.) In order that these five complex amplitudes be determined experimentally at a given energy and angle, in principle, at least nine linearly independent observables (such as differential cross section, polarization, and rotation parameters) must be measured to solve for nine of the ten real quantities in the five complex amplitudes. (One phase is arbitrary.[2]) Since the experimental error for each measurement is not infinitesimal, and the equations for the observables and amplitudes are bilinear, in practice more than nine experiments must be performed in order to determine the pp scattering amplitudes uniquely.

On the other hand, when one simultaneously analyzes both the pp and pn (collectively NN) amplitudes, there are 10 complex amplitudes to be determined (5 for each isospin state), or 19 independent real numbers. (Again, one phase is arbitrary.[2]) On the basis of interference terms in the pp and pn amplitudes, one can obtain three equations by equating observables to amplitudes for each "set" of measurements.[3] (A set contains a measurement of a pp observable at an angle θ^*, $0 \leqslant \theta^* \leqslant \pi/2$, and pn measurements of the same observables at angles θ^* and $\pi - \theta^*$.)

Thus, one can obtain 21 equations with seven sets of measurements, which, in principle, are more than sufficient to determine the NN amplitudes uniquely.

The advantages are realized experimentally also, since pn and pp measurements can usually be performed on the same experimental setup with a change in either target nucleon or beam nucleon (or both) from proton to neutron or vice versa. One can switch between pp and pn measurements in a short time. With a counter hodoscope or spark chamber setup, one essentially measures the entire angular spectrum simultaneously. Therefore, it is possible to determine the NN scattering amplitudes with little more effort than the individual pp or pn scattering amplitudes alone.

In this experiment the pn and pp polarization parameters were measured at energies from 310 to 700 MeV, and c.m. angles from 30 to 150 deg with the same experimental setup.

II. EXPERIMENTAL METHOD AND APPARATUS

In this experiment the nucleon-nucleon polarization was studied by double scattering. A polarized proton beam was produced by scattering an unpolarized external proton beam from the cyclotron on a carbon target at ±6 deg. The polarization of this beam was determined by means of a second scatter on an identical carbon target and measuring the asymmetry with a pair of counter telescopes at ±6 deg from the second target. By reversal of the first scattering angle, the beam polarization is caused to reverse sign (i.e., partial spin alignment changed from up to down or vice versa). By scattering the polarized beam on a nucleon target, we obtained the NN polarization by measuring, at a given angle, the asymmetry in the NN scattering due to beam polarized up and down, and then dividing this by the absolute value of the beam polarization.

The experimental setup is shown in Fig. 1. The external proton beam from the cyclotron, degraded to the desired energy with copper absorbers, entered the experimental area as shown at the top of the figure. The two bending magnets, B_2 and B_3, bent the beam away from and back toward the beam line, respectively. The beam intersected the original beam line at a carbon target with an angle θ_1. (Due to geometry and the limitations of the maximum field available to those magnets, $\theta_1 \leqslant 12$ deg at 700 MeV, and $\theta_1 \leqslant 14$ deg at energies $\leqslant 600$ MeV.) The scattered (hence polarized) protons passing through the lead defining slit were momentum analyzed (momentum spread $\Delta p/p = 6\%$ FWHM) and finally focused (achromatically) on the second target. Upon reversal of the fields in B_2 and B_3, the angle θ_1 was reversed, and hence the sign of the beam polarization was also reversed. The angle θ_1 was monitored by a pair of split ion chambers; one before and one after the polarizing target ensured that the angle θ_1 was accurate and consistent to ± 0.2 deg.

The polarized beam was monitored by three counters (M_1, M_2, and M_3) in coincidence. Counter M_1 was at the intermediate focus of the beam where the momentum dispersion was maximum; the spatial extent of M_1 limited the momentum dispersion of the beam. Counter M_3, a thin counter close to the second target, selected beam particles going through only the central portion of the target.

The polarized proton beam was kept centered on the beam line by means of split counters S_1 to S_4, located near M_2. They counted the fraction of beam to the left and right of the beam line, and above and below the beam height, in coincidence with the monitor signals.

Counters S_5 and S_6 were located downstream to count the left and right portion of the beam. By slight trimming of the currents in magnets B_4 and B_5, it was possible to keep the left-right counters balanced to within 1% in both sets of split counters, thus ensuring that the beam was on the beam line.

To the left of the target (looking downstream) were 19 scintillation counters, P_1 to P_{19}. They detected charged particles (mainly scattered protons). To the right were counter A_9, 1/2-in. of lead, counters A_1 to A_8, and eight 6-in. thick scintillation counters, N_1 to N_8. These thick counters detected high-energy neutrons (>5 MeV) that deflected protons in the scintillator. The efficiency of these counters[4] was about 15%. They were also used to detect charged particles directly with unit efficiency. During pn runs, A_1 to A_9 were in anticoincidence to veto events in which a proton or a γ ray headed toward the N counters. During pp runs, A_1 to A_8 and the 1/2-in. of lead were removed, and A_9 was put in coincidence to ensure that the N counters would detect only charged particles.

The N counters were shielded on all sides except the front by layers of paraffin, boric acid, lead, and steel totaling 18 to 24 in. thick for minimizing the neutron background.

This second target was a liquid hydrogen or liquid deuterium target of standard LRL design with a 7.5-mil Mylar target flask, 3-3/4 in. diam by 5 in. long. Surrounding the target was a vacuum jacket with a 310-deg window of 25-mil Mylar.

The beam energy was measured by means of a telescope counter with variable thickness of copper absorbers in the beam. The energies, normalized for the center of the second target, and widths (energy spreads) are tabulated in Table I. The approximate beam-intensity ratios at the second target due to beam loss through degrading are also listed.

An event was defined by a coincidence of the monitor counters $M_1M_2M_3 = M$, at least one P counter, at least one N counter, and no anticounter. This system either detected two charged particles (predominantly pp), or one charged and one neutral particle (predominantly pn) in the final state. The count from the particular P and N counters that fired for each event were recorded on a magnetic tape through an on-line PDP-5 computer. Six types of runs were made at each energy for both pp and pn systems: with deuterium (D), hydrogen (H), and empty flask (MT) targets, each with both signs of beam polarization. Thus there was a total of 12 different types of runs at each energy.

The three different target conditions in the pn runs were used for background elimination. The three in the pp runs were for comparison of pp runs in a free and quasi-free proton target.

III. ANALYSIS AND RESULTS

The events of a specific type with only one P and one N counter counting were combined to form a 19×8 array, M(P, N), where M is the number of counts per monitor count in the channel (P, N), $P = 1, \cdots, 19$, and $N = 1, \cdots, 8$. Typical distributions for pn and pp runs at 700 MeV are plotted in Figs. 2 and 3, respectively, for counter N_3. The main peak on the left represents elastic (or quasi-elastic) pn or pp events. The rest is background.

For the pp runs in hydrogen, the "pure" pp events were obtained by making the subtraction H - MT - E, where MT represents the background due to the empty target, and E (extrapolation) is the additional background from inelastic events (see Fig. 3). The background E was determined by starting with the curve from H - MT and subtracting a sufficient number of events from each of the three channels forming the main peak so as to be left with a smooth curve across those three channels and the three channels on each side.

For the pn and pp runs in deuterium, the quasi-elastic peaks have long tails in which backgrounds (mainly pion production) and NN events overlap. We have used the hydrogen-target runs to determine the background contribution from the proton, and to estimate the additional contribution to background from the neutron in the deuterium target. In Table II we have summarized the particular $NN \rightarrow NN\pi$ processes (in which only two particles are detected by the counters) that can be confused with one P or one N events. Weighting the contribution of each interaction by its total cross section,[5] one finds that for pn runs, elimination of the background requires the combination of D - 3/2 H + 1/2 MT. For pp runs with a deuterium target, D - MT - E is required, where E is the same E as was determined for hydrogen runs. Figure 4 shows three different combinations for pn runs in deuterium at 700 MeV. The chosen combination (D - 3/2 H + 1/2 MT) is clearly favored. Since the background is very small, the maximum differences of various combinations is only a 2% effect on the asymmetry calculation.

The two-body background reactions in pp interactions, such as $pd \rightarrow pd$ or $pp \rightarrow \pi^+ d$, have very negligible cross sections and most of them do not overlap with the elastic peak. There is no background contribution in pn interactions from two-body final states.

After the above-mentioned background corrections were applied, the three bins with the maximum number of events were summed, and the asymmetry was calculated. Histograms for 700-MeV pn (deuterium) and pp (hydrogen) runs in counter N_3 are shown in Figs. 5 and 6, respectively. In each figure the histogram on the right is the Monte-Carlo calculated distribution with the input of experimental condition of the beam, target, and counter information. With pn runs, the target neutron is approximated by a "free" neutron moving with a Hulthén distribution.[6] For pp runs (Fig. 6), the Monte-Carlo distribution agrees in shape with the measured distribution. The pn Monte-Carlo distribution (Fig. 5) is shifted slightly to the left of the experimental distribution; this may be due to the off-mass shell effect of the target nucleon, or the binding effect of the spectator proton.

Because of the finite angular acceptance of the first scattering angle by the slit, the beam spot at the final target was not symmetrical in either spatial or angular distribution. This lack of symmetry is caused by the sharp forward peaking of the angular distribution of the proton in pC scattering. For example, at 725 MeV the data of McManigal et al.[7] indicate that the differential cross section at 7 deg is twice that at 5 deg. The spatial and angular distribution of the beam at the final target were not measured in this experiment. By assuming the worst possible conditions, and making Monte-Carlo calculations, one can place an upper limit on the false scattering asymmetries arising from beam asymmetries. The maximum error in the scattering asymmetry from these calculations is about 10% in N_1 and N_8 for pp, about 5% in N_8 for pn, and negligible for all the other channels.

The beam polarization was determined to within ±3%. This uncertainty dictates the maximum uncertainty in overall normalization.

The asymmetry and polarization for each neutron counter were calculated in the usual manner. The asymmetry is given by the expression $\epsilon(N) = [L(N) - R(N)]/[L(N) + R(N)]$, where N is a given neutron counter, and L(N) [R(N)] is the number of background subtracted counts mentioned earlier in this section for the first scatter to the left [right]. The polarization for neutron counter N is $P(N) = \epsilon(N)/P_B$ where P_B equals the beam polarization measured in this experiment (described in Sec. II).

Since each neutron counter is located at a fixed laboratory angle, its corresponding c. m. angle and spread in FWHM is calculated by the Monte Carlo method mentioned previously. For pp calculations, since $P(\theta^*)$ is antisymmetrical about $\theta^* = \pi/2$, the data for those neutron counters (i.e., $N \geqslant 5$) corresponding to $\theta^* > \pi/2$ have been altered in the following way. The angle has been changed to its complementary angle (i.e., $\theta^* \rightarrow \pi - \theta^*$) and the sign of polarization reversed.

Polarization parameters for pn and pp runs are tabulated in Tables III and IV, and are plotted in Figs. 7 and 8.

IV. DISCUSSION

It is interesting to observe that the energy dependence of the NN polarization parameter $P^{NN}(\theta^*)$ is small and linear for pn and nearly linear for pp scattering (Figs. 9 and 10). Thus it is possible to parameterize the NN polarization data in the following simple form:

$$P^{NN}(\theta^*, E) = \sin\theta^* \sum_{n,\ell} a_{n\ell} E^n P_\ell(\cos\theta^*),$$

where E is the beam kinetic energy (in BeV), θ^* is the c.m. scattering angle, and P_ℓ is the Legendre polynomial. For our results the parameters $a_{n\ell}$ are as follows:

(1) pn results: number of degrees of freedom (d) = 32 and $\sqrt{\chi^2/d} = 1.19$

$a_{00} = 0.074 \pm 0.023$ | $a_{10} = -0.172 \pm 0.043$
$a_{01} = 0.437 \pm 0.062$ | $a_{11} = 0.056 \pm 0.112$
$a_{02} = 0.356 \pm 0.066$ | $a_{12} = 0.164 \pm 0.124$
$a_{03} = 0.114 \pm 0.092$ | $a_{13} = -0.256 \pm 0.175$

(2) pp results: data for both pp in (H_2) and pp in (D_2)

$d = 59$, $\sqrt{\chi^2/d} = 1.28$

$a_{01} = 0.295 \pm 0.283$ | $a_{11} = 1.971 \pm 1.104$ | $a_{21} = 1.033 \pm 1.040$
$a_{03} = -0.543 \pm 0.438$ | $a_{13} = 3.283 \pm 1.733$ | $a_{23} = -3.347 \pm 1.649$
$a_{05} = -0.002 \pm 0.328$ | $a_{15} = -0.196 \pm 1.359$ | $a_{25} = 0.534 \pm 1.342$

The plots for the fitted results are shown in Figs. 9 and 10.

Although the pn differential cross section I_0^{pn} is known at only a few energies in this region, it is possible to get some I = 0, I_0, and P results from the pp and pn data in existence, by means of the following formulae:

$$I_0^{I=0}(\theta^*) = 2[I_0^{pn}(\theta^*) + I_0^{pn}(\pi - \theta^*)] - I_0^{pp}(\theta^*)$$

$$I_0P^{I=0}(\theta^*) = 2[I_0P^{pn}(\theta^*) - I_0P^{pn}(\pi - \theta^*)] - I_0P^{pp}(\theta^*)$$

$$P^{I=0}(\theta^*) = I_0P^{I=0}(\theta^*)/I_0^{I=0}(\theta^*),$$

where $0 \leq \theta^* \leq \pi/2$.

The angular distributions of $I_0^{I=0}$ and $P^{I=0}$ vs $\cos\theta^*$ for 350, 500, and 630 MeV at which the pn differential cross sections have been measured[8] are shown in Fig. 11.

Because seven "sets" (see Sec. I) of pp and pn parameters are required to determine the nucleon-nucleon scattering amplitudes, these data represent only a partial contribution toward the determination of these amplitudes. However, the results of this experiment show that the deuteron can be used as a good neutron target at high energies, provided some precautions are taken. Furthermore, since this experiment shows that the pn polarization is quite large at these energies, it should be possible to perform the more difficult triple-scattering experiments in the pn system, and the measurement of the D, R, and R' parameters for both pp and pn systems have been scheduled for the 184-inch cyclotron in the near future.

ACKNOWLEDGMENTS

We are greatly indebted to Professors B. J. Moyer and A. C. Helmholz and other members of their research group for assistance in this experiment. The assistance from other sections of the Lawrence Radiation Laboratory, such as the electronics groups, the computer center staff, and the 184-in. cyclotron crew, is greatly appreciated also. Of special note is the help received from William P. Oliver, Narender Sehgal, and Kenneth Caproni in the running of the experiment.

APPENDIX

The scattering matrix for the two-nucleon system, when spatial rotational invariance, parity conservation, time reversal invariance and charge independence are assumed, can be written as[1]

$$M = a + ic(\sigma_{1n} + \sigma_{2n}) + m\,\sigma_{1n}\sigma_{2n} + (g+h)\,\sigma_{1\ell}\sigma_{2\ell} + (g-h)\,\sigma_{1m}\sigma_{2m},$$

where

$$\sigma_{ik} = \underset{\sim}{\sigma}_i \cdot \underset{\sim}{k} ,$$

$\underset{\sim}{\sigma}_i$ is the Pauli spinor for particle i(i = 1, 2) in either the initial or the final system, and $\hat{k}$ is a unit vector which takes the following three orthogonal directions $\hat{n}$, $\hat{\ell}$, or $\hat{m}$.

$\hat{n} = (\underset{\sim}{k}_i \times \underset{\sim}{k}_f)/|\underset{\sim}{k}_i \times \underset{\sim}{k}_f|$ is the normal of the scattering plane, $\underset{\sim}{k}_i$ and $\underset{\sim}{k}_f$ are the initial and final momenta for either particle 1 or particle 2, respectively, in the c.m. system.

$\hat{\ell} = (\underset{\sim}{k}_i + \underset{\sim}{k}_f)/|\underset{\sim}{k}_i + \underset{\sim}{k}_f|$. In the non-relativistic case for scattering two particles of identical mass, $\hat{\ell}$ is in the direction of final momentum in the laboratory system.

$\hat{m} = (\underset{\sim}{k}_f - \underset{\sim}{k}_i)/|\underset{\sim}{k}_f - \underset{\sim}{k}_i|$ is a unit vector perpendicular to both $\hat{n}$ and $\hat{\ell}$, and the three directions are mutually perpendicular and form a right-handed coordinate system.

For a given interaction (i.e., pp, pn, or nn), the coefficients a, c, m, g, and h are the five complex (Wolfenstein) amplitudes (functions of E and θ^*) with names such as non-spin flip, one-spin flip, and double-spin flip associated with them.

FOOTNOTES AND REFERENCES

*Work supported by the U. S. Atomic Energy Commission.

†Present address: Virginia Polytechnic Institute, Blacksburg, Virginia.

1. L. Wolfenstein and J. Ashkins, Phys. Rev. 85, 947 (1952).

2. The overall phase is not determined from this formalism because the amplitudes are bilinear in the observables. However, the phase can be determined from the optical theorem relating the imaginary part of the scattering amplitude to the total cross section.

3. B. M. Golovin, V. P. Dzhelopov, V. S. Nadezhdin, and V. I. Sataro, J. Exptl. Theoret. Phys. 36, 433-443 (1959); (English translation) Sov. Phys. JETP 9, 302 (1959).

4. R. J. Kurz, A 709/7090 FORTRAN II Program to Compute the Neutron-Detection Efficiency of Plastic Scintillator for Neutron Energies from 1 to 300 MeV, Lawrence Radiation Laboratory Report UCRL-11339, 1964 (unpublished).

5. W. O. Lock, High Energy Nuclear Physics (John Wiley and Sons, Inc., New York, 1960). Chap. VIII, pp. 161-179.

6. L. Hulthén and M. Sugawara, Encyclopedia of Physics, XXXIX (Springer Verlag, Berlin, 1957).

7. P. G. McManigal, R. D. Eandi, S. N. Kaplan, and B. J. Moyer, Phys. Rev. 137, B620 (1965).

8. The data at 350, 500, and 630 MeV are extrapolated from np I_0 measurements to nearby energies both higher and lower. These data were taken from the reference list of the appendix of Richard Wilson's book on The Nucleon-Nucleon Interaction (Interscience Publishers, 1963).

9. R. T. Siegel, A. J. Hartzler, and W. A. Love, Phys. Rev. 101, 838 (1956).

10. O. Chamberlain, E. Segrè, R. D. Tripp, C. Wiegand, and T. Ypsilantis, Phys. Rev. 105, 288 (1957).

11. M. G. Meshcheryakov, S. B. Nurshev, and G. D. Stoletov, J. Exptl. Theoret. Phys. 33, 37-45 (1957), (English translation) Sov. Phys. JETP 6, 28 (1958).

Table I. Beam energies and intensities at the center of the second target.

Beam (MeV)	Measured energy (MeV)	Cu degrader thickness (inches)	Approximate intensity ratio[a]
310	307 ± 11	8 13/16	0.0022
400	394 ± 12	7 1/4	0.0035
500	498 ± 11	5 1/16	0.0046
600	601 ± 9	2 7/16	0.0071
700	702 ± 5	0	1.0000

a. For explanation, see text.

Table II. Background contribution from $NN \rightarrow NN\pi$ in LH_2 and LD_2 targets.

Target	Process	Final state: 1 neutron + 1 charged particle	Final state: 2 charged particles	Total cross section (mb) at following energies (MeV): 400	500	600	700
D, H	$pp \rightarrow pp\pi^0$		X	0.06	0.5	2.0	4.0
D, H	$pp \rightarrow pn\pi^+$	X	X	0.4	3.5	7.0	12.0
D	$pn \rightarrow pn\pi^0$	X		0.2	1.5	2.5	4.0
D	$pn \rightarrow pp\pi^-$		X	0.03	0.3	1.0	2.0
D	$pn \rightarrow nn\pi^+$	X		0.03	0.3	1.0	2.0
Summary for pn		ΣH		0.4	3.5	7.0	12.0
		ΣD		0.63	5.3	10.5	18.0
		$\Sigma D/\Sigma H$		1.6	1.5	1.5	1.5
Summary for pp			ΣH	0.46	4.0	9.0	16.0
			ΣD	0.49	4.3	10.0	18.0
			$\Sigma D/\Sigma H$	1.1	1.1	1.1	1.1

Table III. Polarization parameters in the pn system. (Overall normalization uncertainty is <3%. Errors shown are due to statistics only.)

Beam energy and polarization	θ^* (deg)	ϵ (%)	P
700 MeV	29.5 ± 6.7	9.15 ± 0.75	0.334 ± 0.027
P_B = 0.274	44.3 ± 6.7	8.36 ± 0.46	0.305 ± 0.017
	60.4 ± 6.5	4.29 ± 0.91	0.157 ± 0.033
	77.1 ± 6.0	-1.86 ± 0.81	-0.068 ± 0.030
	93.8 ± 5.7	-9.65 ± 0.72	-0.352 ± 0.026
	110.9 ± 5.4	-11.27 ± 0.87	-0.411 ± 0.032
	127.1 ± 5.3	-6.78 ± 0.53	-0.247 ± 0.019
	143.2 ± 4.9	-3.99 ± 0.52	-0.146 ± 0.019
600 MeV	33.0 ± 6.0	11.49 ± 1.26	0.364 ± 0.040
P_B = 0.316	48.5 ± 5.8	7.92 ± 1.30	0.251 ± 0.041
	64.8 ± 5.6	2.67 ± 0.96	0.084 ± 0.030
	81.3 ± 5.7	-4.90 ± 0.88	-0.155 ± 0.028
	97.8 ± 5.6	-9.95 ± 0.99	-0.315 ± 0.031
	114.7 ± 5.6	-10.89 ± 0.96	-0.345 ± 0.030
	130.5 ± 5.6	-7.61 ± 0.74	-0.241 ± 0.023
	145.6 ± 5.1	-2.85 ± 0.73	-0.090 ± 0.023
500 MeV	33.4 ± 5.8	10.23 ± 0.82	0.297 ± 0.024
P_B = 0.345	48.5 ± 6.1	8.79 ± 0.54	0.255 ± 0.016
	64.7 ± 5.9	3.11 ± 0.57	0.090 ± 0.017
	81.2 ± 5.9	-5.35 ± 0.60	-0.155 ± 0.017
	97.9 ± 5.9	-9.11 ± 0.62	-0.264 ± 0.018
	115.0 ± 5.9	-9.08 ± 0.60	-0.263 ± 0.017
	130.9 ± 5.7	-5.06 ± 0.59	-0.147 ± 0.017
	145.2 ± 4.9	-3.82 ± 0.60	-0.111 ± 0.017

Table III. (cont.)

Beam energy and polarization	θ^* (deg)	ϵ (%)	P
400 MeV	33.1 ± 6.9	15.70 ± 3.31	0.411 ± 0.087
P_B = 0.382	48.3 ± 6.9	10.10 ± 0.86	0.264 ± 0.023
	66.6 ± 7.2	3.18 ± 1.24	0.083 ± 0.032
	83.1 ± 7.0	-5.80 ± 0.98	-0.152 ± 0.026
	99.7 ± 6.8	-11.82 ± 0.94	-0.309 ± 0.025
	116.5 ± 6.6	-10.40 ± 0.83	-0.272 ± 0.022
	131.1 ± 5.9	-6.02 ± 0.69	-0.158 ± 0.018
	144.3 ± 5.1	-3.97 ± 2.14	-0.104 ± 0.056
310 MeV	33.1 ± 6.7	18.00 ± 1.61	0.421 ± 0.038
P_B = 0.428	47.8 ± 7.2	12.27 ± 1.11	0.287 ± 0.026
	66.7 ± 8.1	3.96 ± 0.85	0.093 ± 0.020
	83.2 ± 8.0	-4.87 ± 1.02	-0.114 ± 0.024
	99.8 ± 7.8	-10.22 ± 0.80	-0.239 ± 0.019
	116.5 ± 7.6	-9.31 ± 0.69	-0.218 ± 0.016
	130.7 ± 6.8	-7.45 ± 0.75	-0.174 ± 0.018
	141.5 ± 7.2	-5.68 ± 1.32	-0.133 ± 0.031

θ^* = proton scattering angle in c. m. ϵ = asymmetry

P = polarization

Table IV(a). pp polarization in LH_2 target. (Overall normalization uncertainty is less than 3%. Errors shown are due to statistics only.

Beam energy and polarization	θ^*(deg)	ϵ(%)	P	P/sin θ^*
700 MeV	30.8 ± 1.7	15.2 ± 0.52	0.555 ± 0.019	1.083 ± 0.037
P_B = 0.274	35.7 ± 1.7	14.3 ± 0.33	0.522 ± 0.012	0.894 ± 0.021
	43.2 ± 3.5	15.3 ± 0.44	0.558 ± 0.016	0.816 ± 0.023
	52.4 ± 3.1	14.5 ± 0.61	0.529 ± 0.022	0.668 ± 0.028
	60.1 ± 3.6	13.0 ± 0.30	0.474 ± 0.011	0.547 ± 0.013
	68.7 ± 3.3	9.7 ± 1.08	0.354 ± 0.039	0.380 ± 0.042
	77.0 ± 3.6	7.0 ± 0.42	0.255 ± 0.015	0.262 ± 0.016
	86.1 ± 3.5	3.0 ± 1.04	0.109 ± 0.038	0.110 ± 0.038
600 MeV	33.6 ± 2.5	16.2 ± 0.31	0.513 ± 0.010	0.926 ± 0.018
P_B = 0.316	34.5 ± 1.5	18.8 ± 1.10	0.595 ± 0.035	1.059 ± 0.061
	46.1 ± 3.6	16.3 ± 0.32	0.516 ± 0.010	0.716 ± 0.014
	49.5 ± 3.2	15.3 ± 0.32	0.484 ± 0.010	0.637 ± 0.013
	63.1 ± 3.6	12.6 ± 0.61	0.399 ± 0.019	0.446 ± 0.022
	65.6 ± 3.4	11.4 ± 1.20	0.361 ± 0.038	0.396 ± 0.042
	80.2 ± 3.6	5.3 ± 0.32	0.168 ± 0.010	0.170 ± 0.010
	82.9 ± 3.5	3.6 ± 0.79	0.114 ± 0.025	0.115 ± 0.025
500 MeV	33.7 ± 2.3	16.9 ± 0.38	0.490 ± 0.011	0.883 ± 0.020
P_B = 0.345	36.8 ± 1.0	17.6 ± 2.03	0.510 ± 0.059	0.852 ± 0.098
Norm. error	46.9 ± 3.6	15.9 ± 0.61	0.461 ± 0.018	0.631 ± 0.024
1.4%	48.7 ± 3.1	15.6 ± 0.49	0.452 ± 0.014	0.602 ± 0.019
	64.1 ± 3.6	9.3 ± 0.35	0.270 ± 0.010	0.300 ± 0.011
	64.6 ± 3.3	10.8 ± 0.87	0.313 ± 0.025	0.347 ± 0.028
	81.3 ± 3.6	3.7 ± 0.52	0.107 ± 0.015	0.108 ± 0.015
	81.8 ± 3.5	3.9 ± 0.55	0.113 ± 0.016	0.114 ± 0.016

Table IV(a). (cont.)

Beam energy and polarization	θ^* (deg)	ϵ (deg)	P	$P/\sin\theta^*$
400 MeV	33.8 ± 2.3	16.9 ± 0.52	0.442 ± 0.014	0.795 ± 0.024
P_B = 0.382	47.8 ± 3.1	16.0 ± 0.29	0.419 ± 0.008	0.565 ± 0.010
	48.0 ± 3.6	16.0 ± 0.41	0.419 ± 0.011	0.564 ± 0.014
	63.5 ± 3.3	10.5 ± 0.30	0.275 ± 0.008	0.307 ± 0.009
	65.2 ± 3.7	10.4 ± 0.37	0.272 ± 0.010	0.300 ± 0.011
	80.6 ± 3.5	4.0 ± 0.32	0.105 ± 0.008	0.106 ± 0.008
	82.5 ± 3.7	3.2 ± 0.33	0.084 ± 0.009	0.084 ± 0.009
310 MeV	33.6 ± 2.4	17.2 ± 1.05	0.402 ± 0.025	0.726 ± 0.044
P_B = 0.428	47.3 ± 2.8	16.0 ± 0.31	0.374 ± 0.007	0.509 ± 0.010
	50.1 ± 2.7	15.5 ± 0.49	0.362 ± 0.011	0.472 ± 0.015
	62.4 ± 3.2	11.8 ± 0.30	0.276 ± 0.007	0.311 ± 0.008
	66.3 ± 3.7	9.3 ± 0.35	0.217 ± 0.008	0.237 ± 0.009
	79.4 ± 3.5	5.0 ± 0.30	0.117 ± 0.007	0.119 ± 0.007
	83.7 ± 3.6	1.5 ± 0.35	0.035 ± 0.008	0.035 ± 0.008

Table IV(b). pp polarization in LD_2 target. (Overall normalization uncertainty is less than 3%. Errors shown are due to statistics only.)

Beam energy and polarization	θ^* (deg)	ϵ (%)	P	P/sin θ^*
700 MeV	29.5 ± 6.7	11.6 ± 1.41	0.423 ± 0.051	0.860 ± 0.105
P_B = 0.274	36.8 ± 4.9	13.4 ± 0.88	0.489 ± 0.032	0.816 ± 0.054
	44.3 ± 6.7	14.7 ± 0.67	0.536 ± 0.024	0.768 ± 0.035
	52.9 ± 5.2	13.7 ± 0.05	0.500 ± 0.018	0.627 ± 0.023
	60.4 ± 6.5	11.7 ± 0.76	0.427 ± 0.028	0.491 ± 0.032
	69.1 ± 5.4	11.5 ± 0.73	0.420 ± 0.027	0.449 ± 0.029
	77.1 ± 6.0	6.2 ± 0.76	0.266 ± 0.028	0.232 ± 0.028
	86.2 ± 5.7	3.5 ± 0.99	0.128 ± 0.036	0.128 ± 0.036
600 MeV	33.0 ± 6.0	16.9 ± 2.45	0.535 ± 0.078	0.982 ± 0.142
P_B = 0.316	34.4 ± 5.1	15.0 ± 1.29	0.475 ± 0.041	0.840 ± 0.072
	48.5 ± 5.8	17.6 ± 1.26	0.557 ± 0.040	0.744 ± 0.053
	49.5 ± 5.6	14.2 ± 0.67	0.449 ± 0.021	0.591 ± 0.028
	64.8 ± 5.6	11.8 ± 0.91	0.373 ± 0.029	0.413 ± 0.032
	65.3 ± 5.6	10.6 ± 0.32	0.335 ± 0.010	0.369 ± 0.011
	81.3 ± 5.7	3.9 ± 0.85	0.123 ± 0.027	0.125 ± 0.027
	82.2 ± 5.6	4.5 ± 0.82	0.142 ± 0.026	0.144 ± 0.026
500 MeV	33.4 ± 5.8	17.5 ± 2.31	0.507 ± 0.067	0.921 ± 0.122
P_B = 0.345	48.5 ± 6.1	14.7 ± 1.16	0.426 ± 0.034	0.569 ± 0.045
	49.1 ± 5.7	14.2 ± 0.73	0.412 ± 0.021	0.545 ± 0.028
	64.7 ± 5.9	9.1 ± 0.78	0.264 ± 0.023	0.292 ± 0.025
	65.0 ± 5.9	9.5 ± 0.68	0.275 ± 0.020	0.304 ± 0.022
	81.2 ± 5.9	4.0 ± 0.74	0.116 ± 0.021	0.117 ± 0.022
	82.1 ± 5.1	3.8 ± 0.71	0.110 ± 0.021	0.111 ± 0.021

Table IV(b). (cont.)

Beam energy and polarization	θ^* (deg)	ϵ (%)	P	P/sin θ^*
400 MeV	33.1 ± 6.9	16.9 ± 2.96	0.442 ± 0.007	0.810 ± 0.142
P_B = 0.382	48.3 ± 6.9	14.8 ± 1.00	0.387 ± 0.026	0.519 ± 0.035
	48.9 ± 6.9	16.0 ± 0.61	0.419 ± 0.016	0.556 ± 0.021
	63.5 ± 6.6	9.4 ± 0.58	0.246 ± 0.015	0.275 ± 0.017
	66.6 ± 7.2	10.3 ± 0.74	0.270 ± 0.019	0.294 ± 0.021
	80.3 ± 6.8	2.9 ± 0.59	0.076 ± 0.015	0.077 ± 0.016
	83.1 ± 7.0	2.4 ± 0.62	0.063 ± 0.016	0.063 ± 0.016

FIGURE CAPTIONS

Fig. 1. Layout of the experimental setup.

Fig. 2. Comparison of pn events in all proton counters for neutron counter N_3 at 700-MeV incident proton energy for three different target conditions: target filled with liquid deuterium, target filled with liquid hydrogen, and target empty. Horizontal lines indicate position of zero counts.

Fig. 3. Comparison of pp events in all proton counters for neutron counter N_3 at 700-MeV incident proton energy for two different target conditions: target filled with liquid hydrogen, target empty, and background extrapolation from off-center peak events under target filled minus target empty.

Fig. 4. Comparison of pn events in all proton counters for N_3 at 700-MeV incident proton energy for different methods of background subtraction (see text). Horizontal lines indicate position of zero counts.

Fig. 5. Comparison of pn events in proton counters for neutron counter N_3 at 700-MeV incident proton energy for beam polarization up and down, and Monte-Carlo calculation simulation of this experiment, assuming the target neutron is moving with just the Hulthén momentum distribution (see text). Horizontal lines indicate position of zero counts.

Fig. 6. Same as Fig. 5 for pp events.

Fig. 7. pn polarization from results of this experiment ( ) plus comparison with other experimental results. Errors are only statistical. Overall normalization uncertainty is less than 3%.

See text for upper limits of systematic errors. (a) 700-MeV incident proton energy; (b) 600 MeV; 635 MeV, from Golovin et al. (Ref. 3); (c) 500 MeV; (d) 400 MeV; (e) 310 MeV; 350 MeV, Siegel et al. (Ref. 9); 310 MeV, Chamberlain et al. (Ref. 10).

Fig. 8. pp polarizations from results of this experiment plus (data taken with hydrogen target, data taken with deuterium target) plus comparisons with other experimental results that do not agree with this experiment. Errors are statistical. Overall normalization uncertainty is less than 3%. See text for upper limits of systematic errors. (a) 700-MeV incident proton energy; (b) 600 MeV; 635 MeV, Meshcheryakov et al. (Ref. 11); (c) 500 MeV; (d) 400 MeV; (e) 310 MeV.

Fig. 9. Fitted curves of pn polarizations from results of this experiment. Note that only small and linear energy dependence is present.

Fig. 10. Same as Fig. 9 for pp results.

Fig. 11. Differential cross sections and polarization results for isospin = 0 NN states at 350, 500, and 630 MeV.

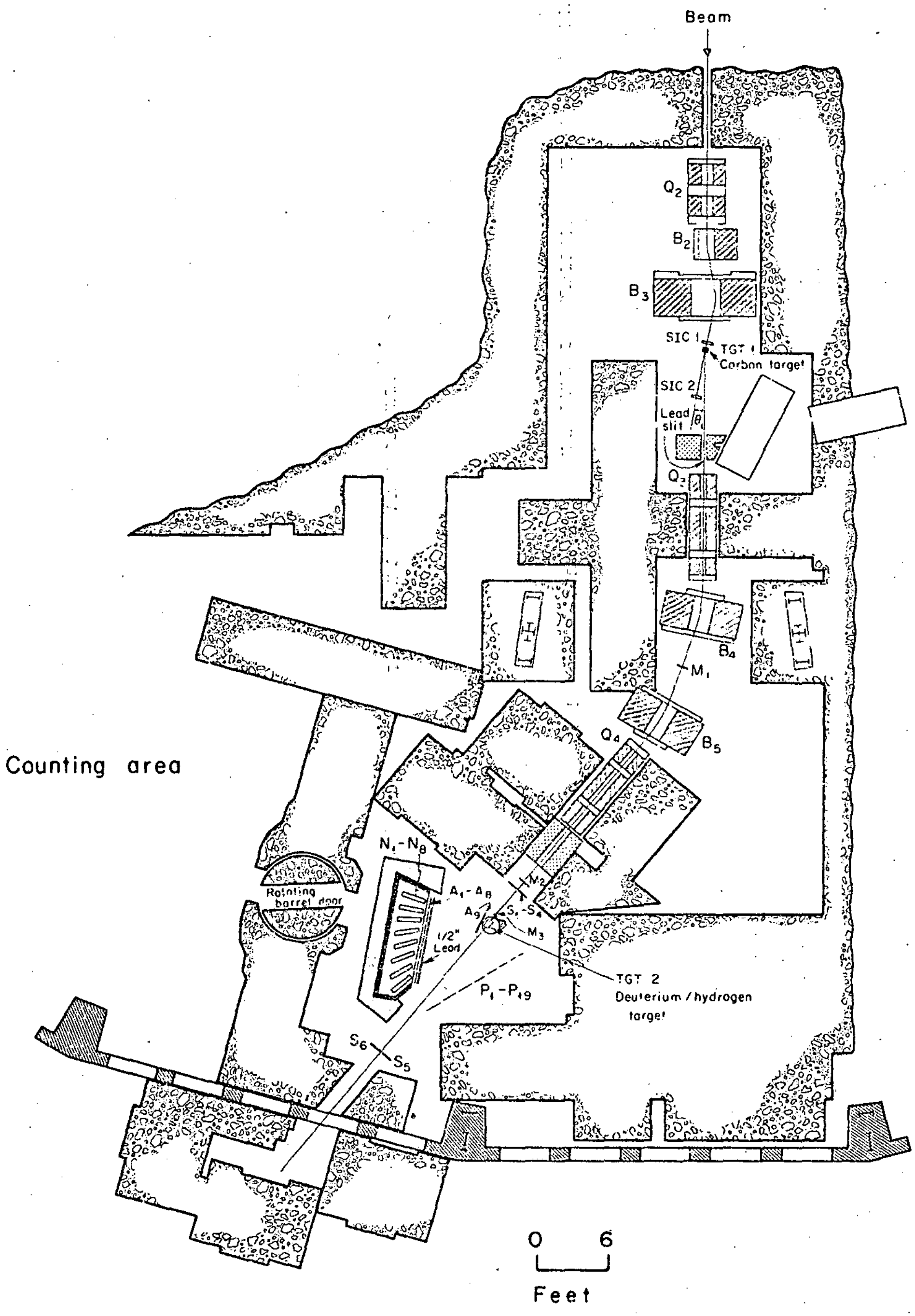

MU-35241

Fig. 1

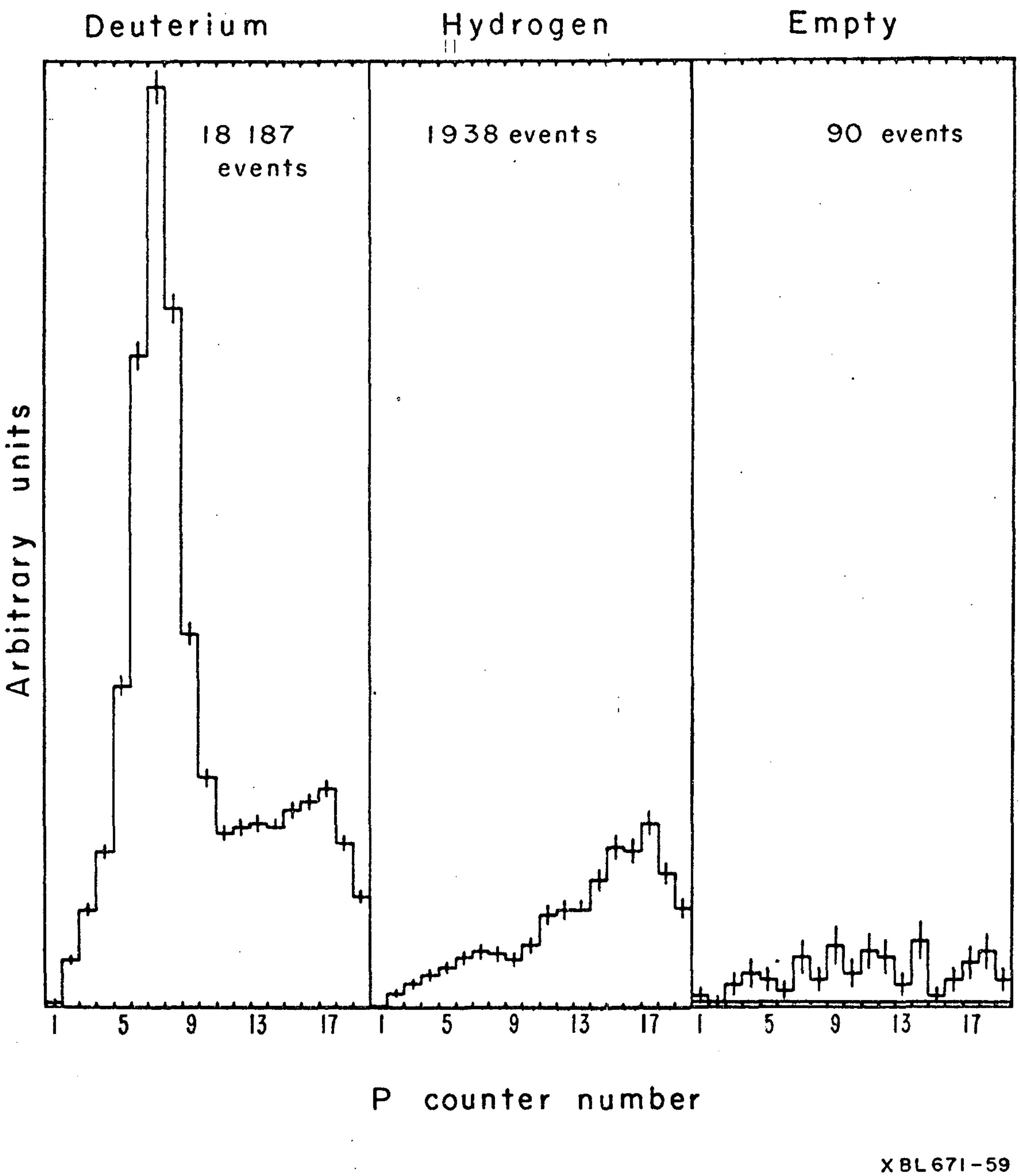
Deuterium
Hydrogen
Empty
18 187
events
1938 events
90 events
Arbitrary units
1
5
9
13
17
P counter number
XBL671-59

Fig. 2

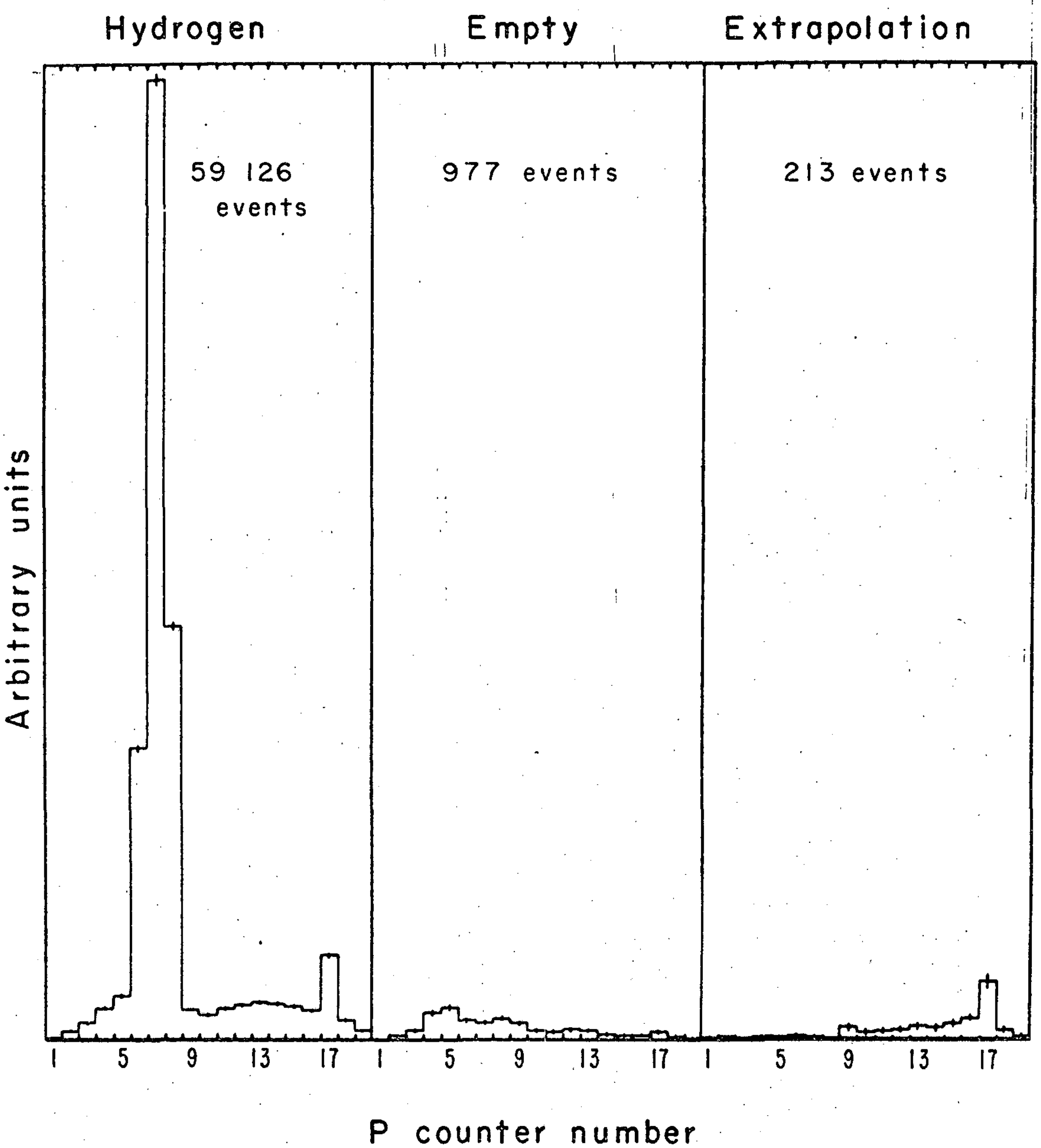

XBL671-57

Fig. 3

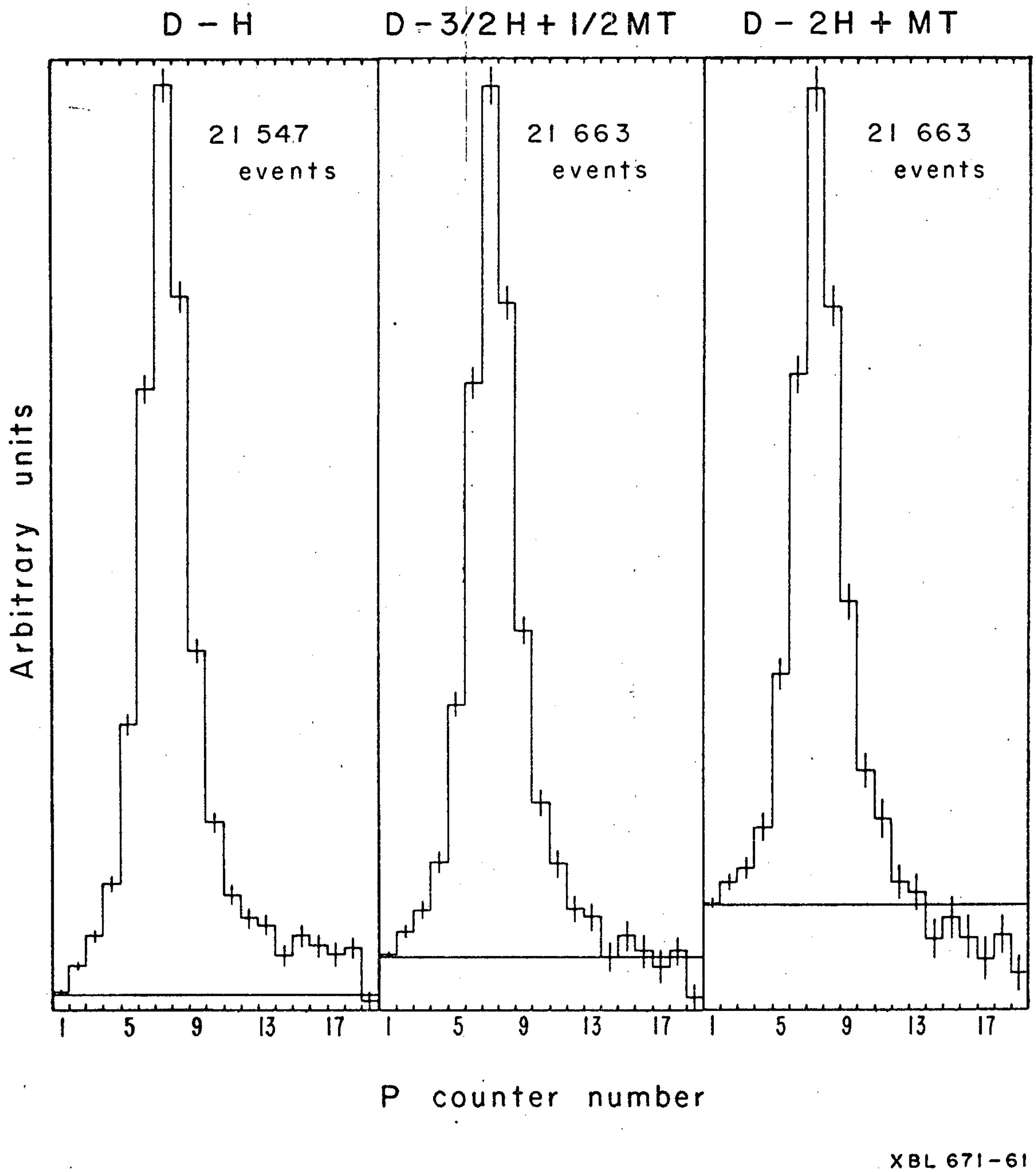
D – H
D – 3/2 H + 1/2 MT
D – 2H + MT
21 547 events
21 663 events
21 663 events
Arbitrary units
1 5 9 13 17
1 5 9 13 17
1 5 9 13 17
P counter number
XBL 671-61

Fig. 4

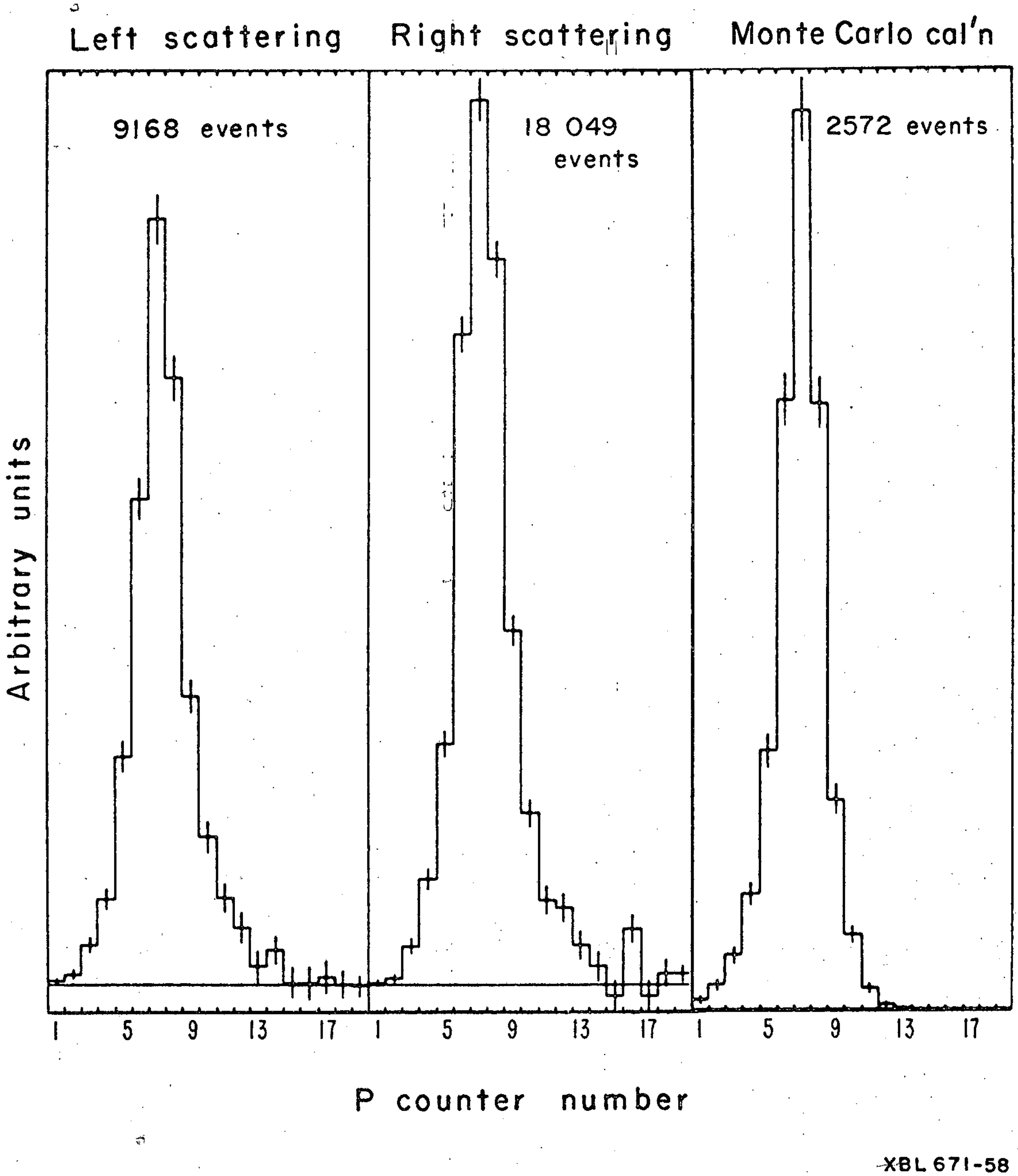

Left scattering
Right scattering
Monte Carlo cal'n
9168 events
18 049 events
2572 events
Arbitrary units
1 5 9 13 17
1 5 9 13 17
1 5 9 13 17
P counter number
XBL 671-58

Fig. 5

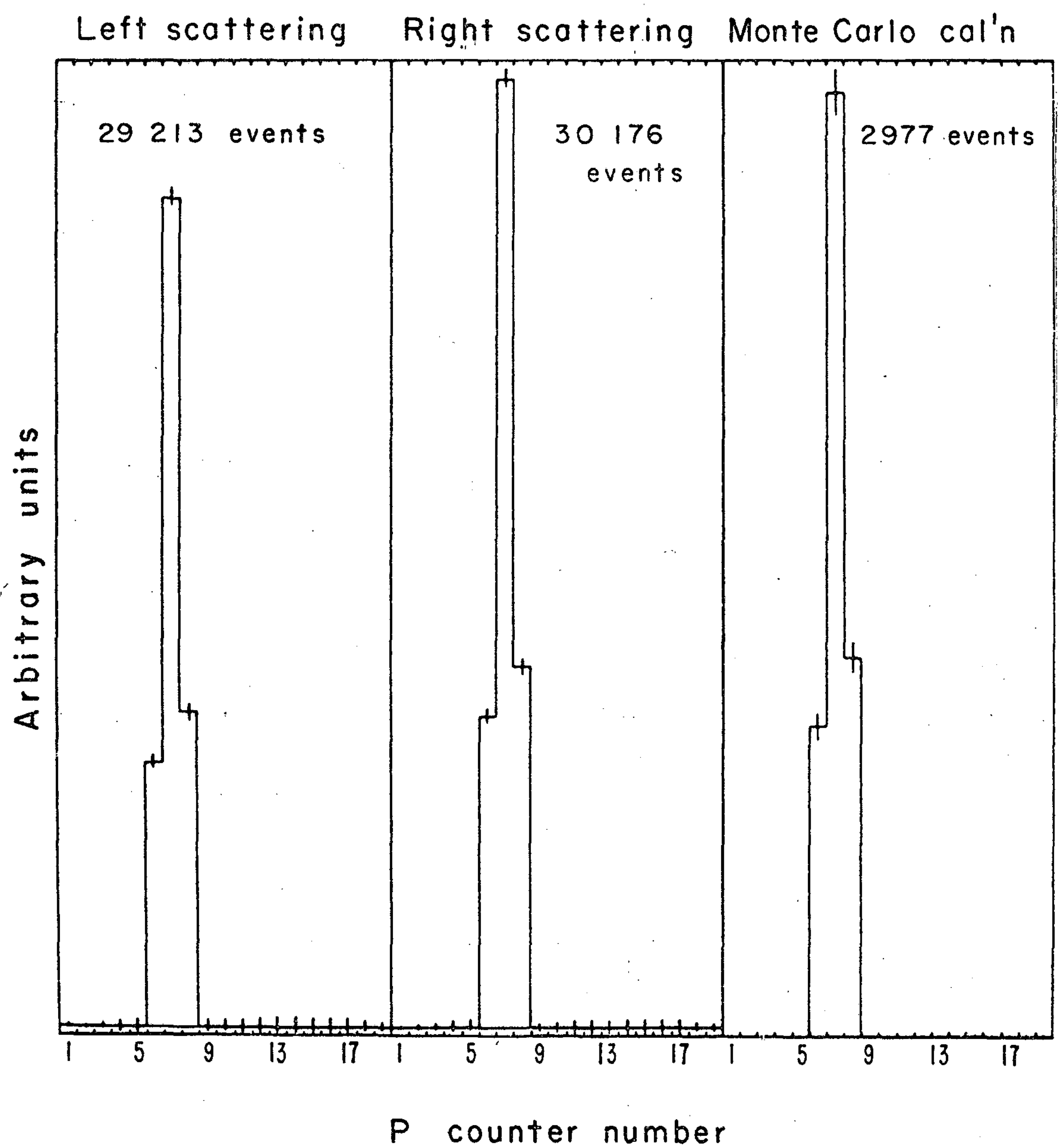
Left scattering
Right scattering
Monte Carlo cal'n
29 213 events
30 176 events
2977 events
Arbitrary units
1
5
9
13
17
P counter number
XBL671-60

Fig. 6

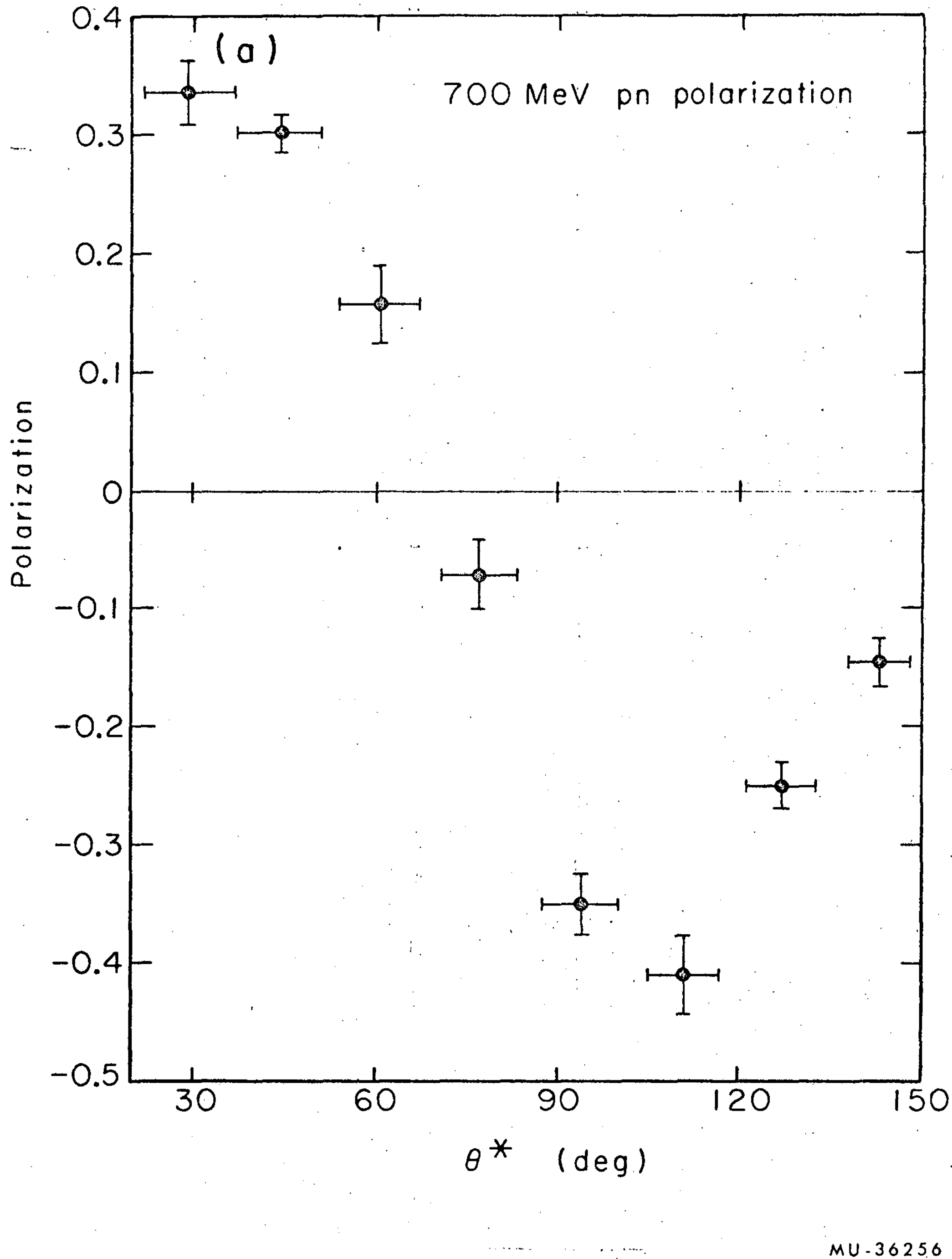
(a)
700 MeV pn polarization
0.4
0.3
0.2
0.1
0
-0.1
-0.2
-0.3
-0.4
-0.5
Polarization
30
60
90
120
150
θ* (deg)
MU-36256

Fig. 7(a)

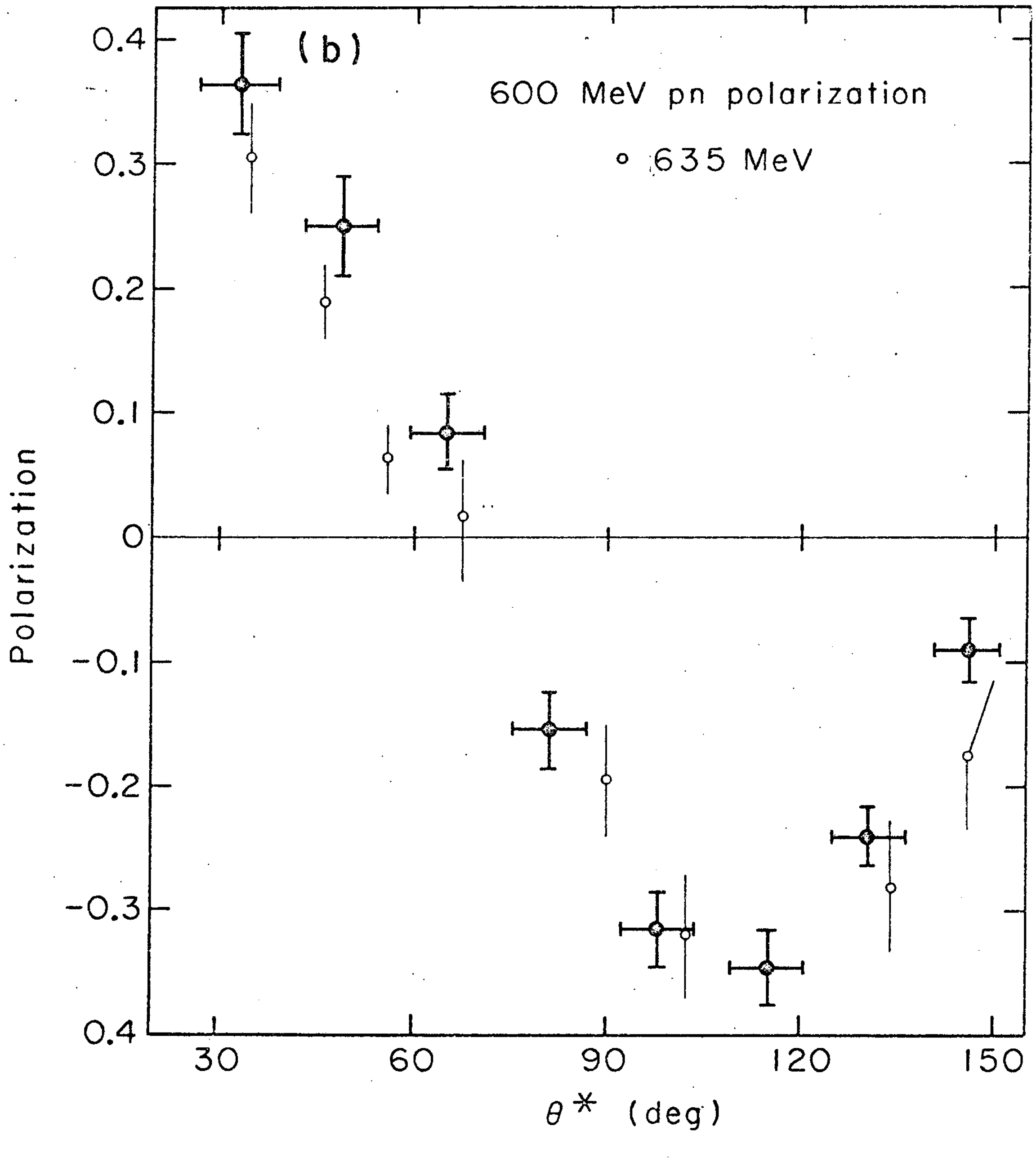

Fig. 7(b) MU-36248

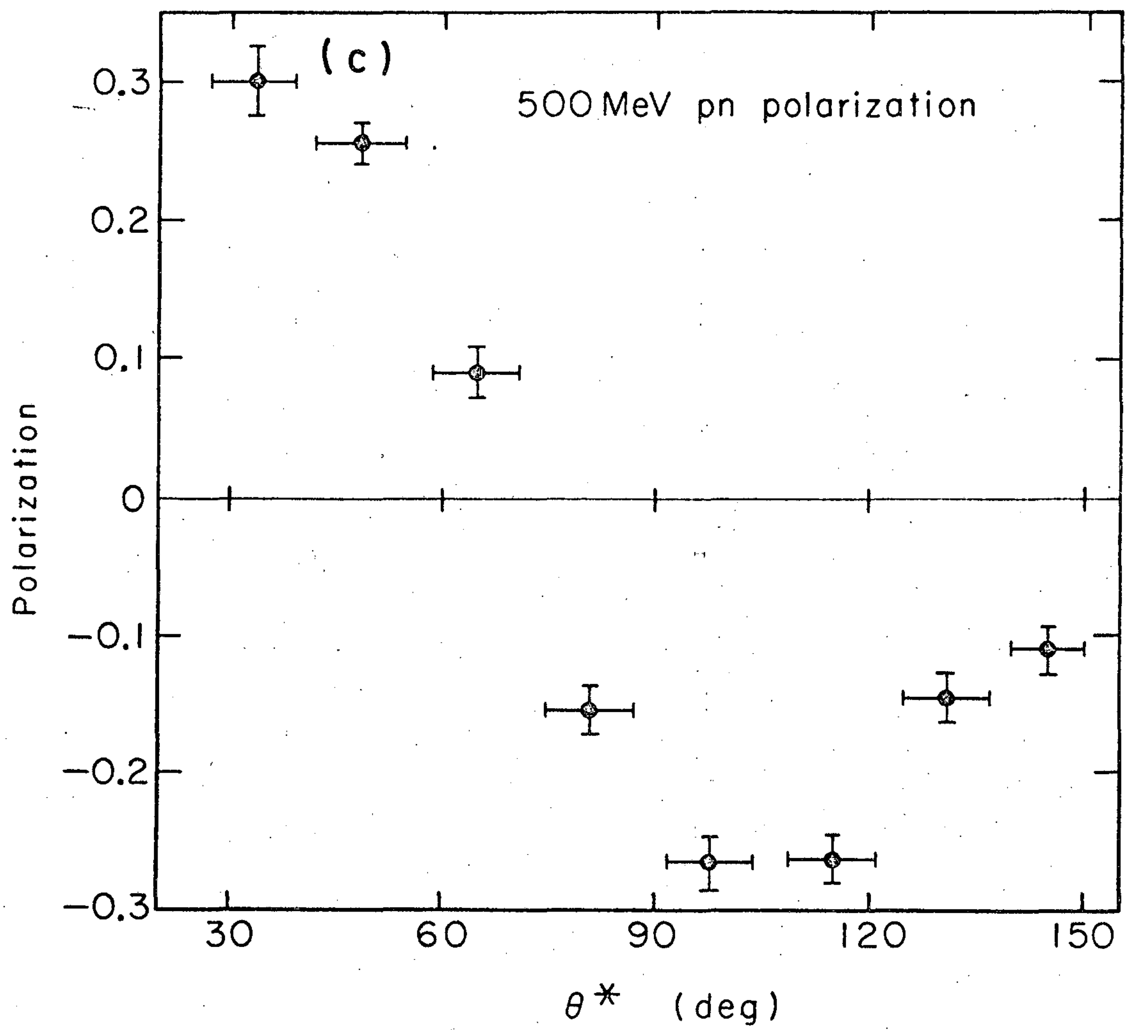
(c)
500 MeV pn polarization
Polarization
0.3
0.2
0.1
0
−0.1
−0.2
−0.3
30
60
90
120
150
θ^* (deg)
MU-36255

Fig. 7(c)

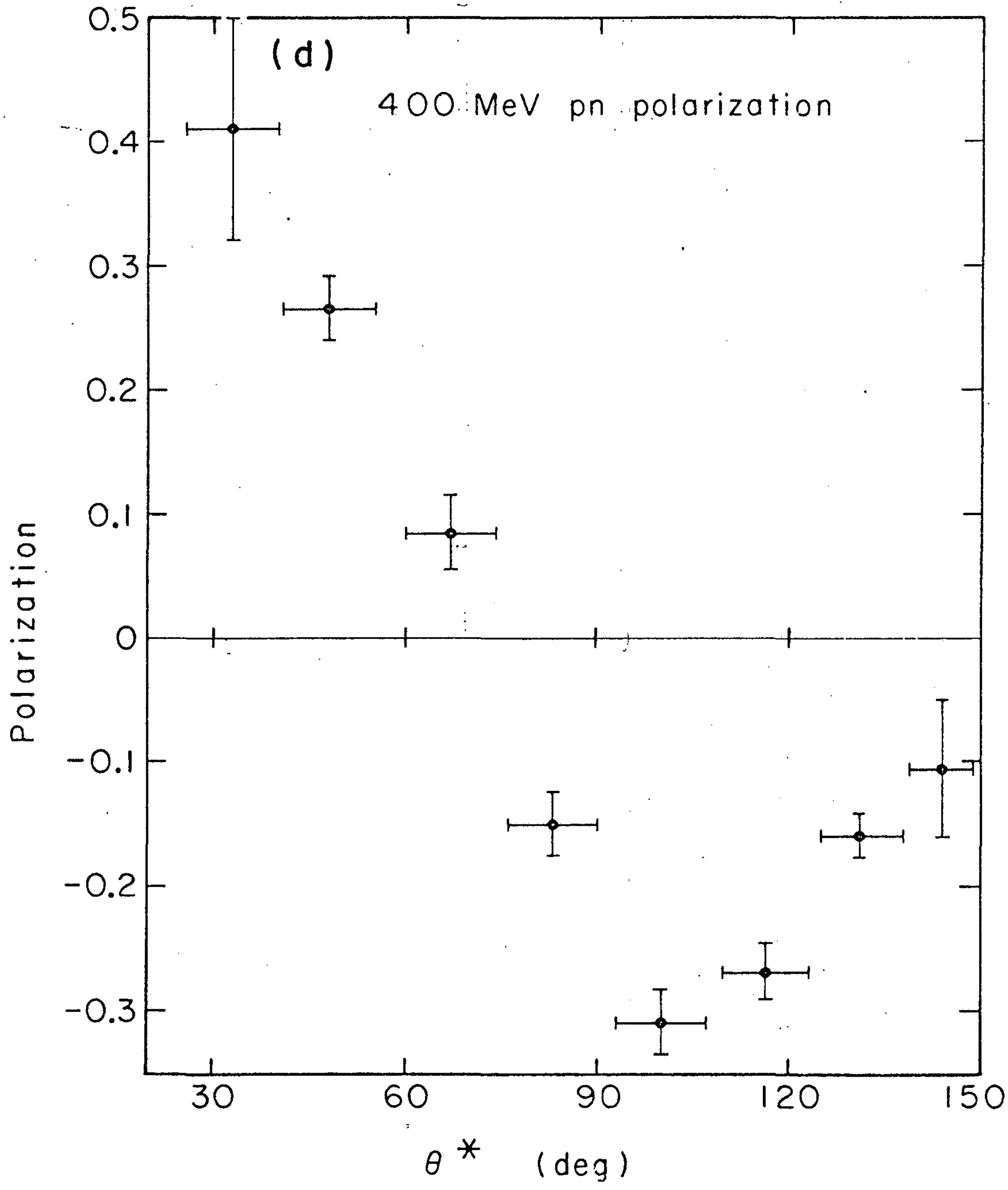

Fig. 7(d)

MU-36243

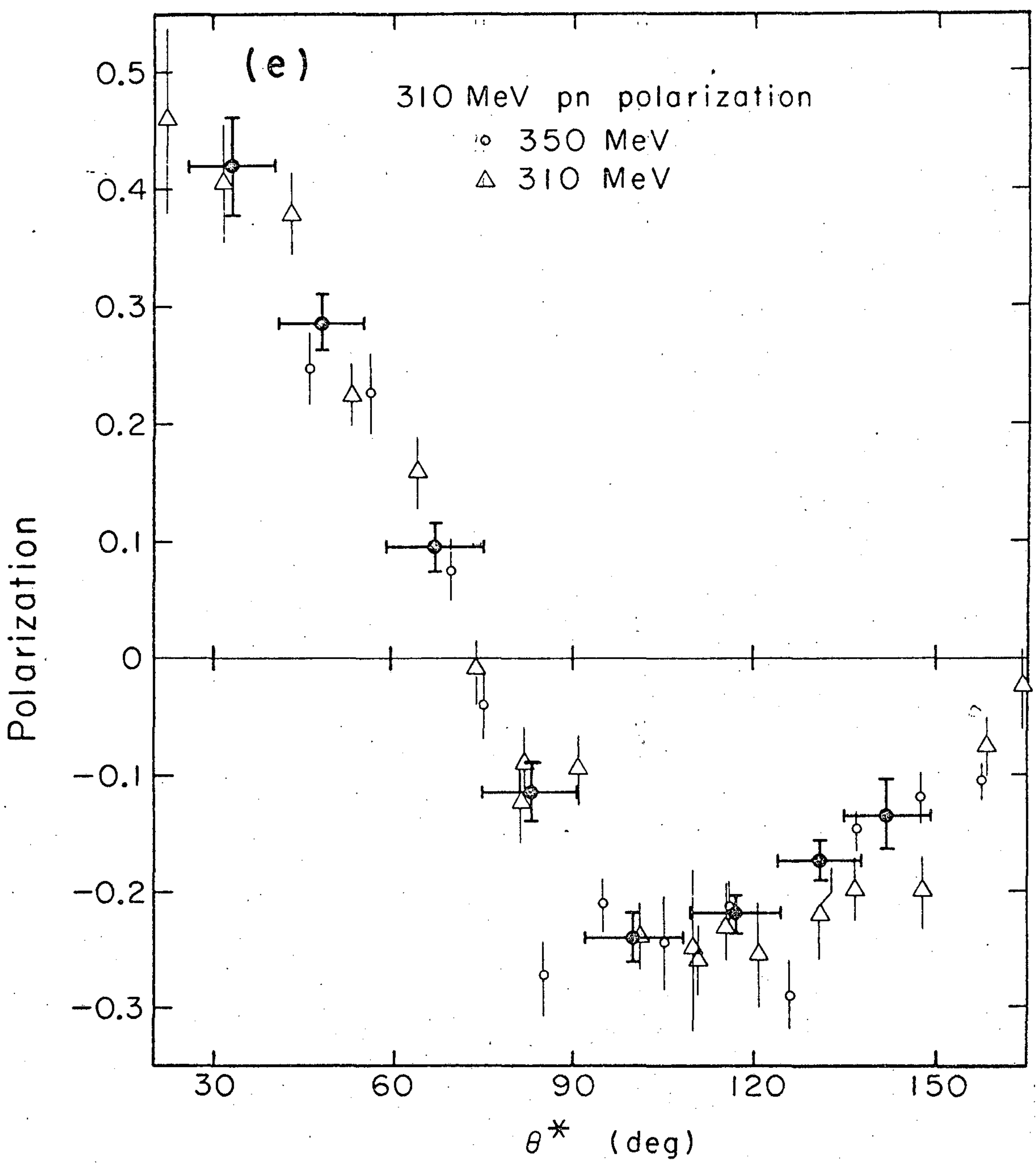

MU-36246

Fig. 7(e)

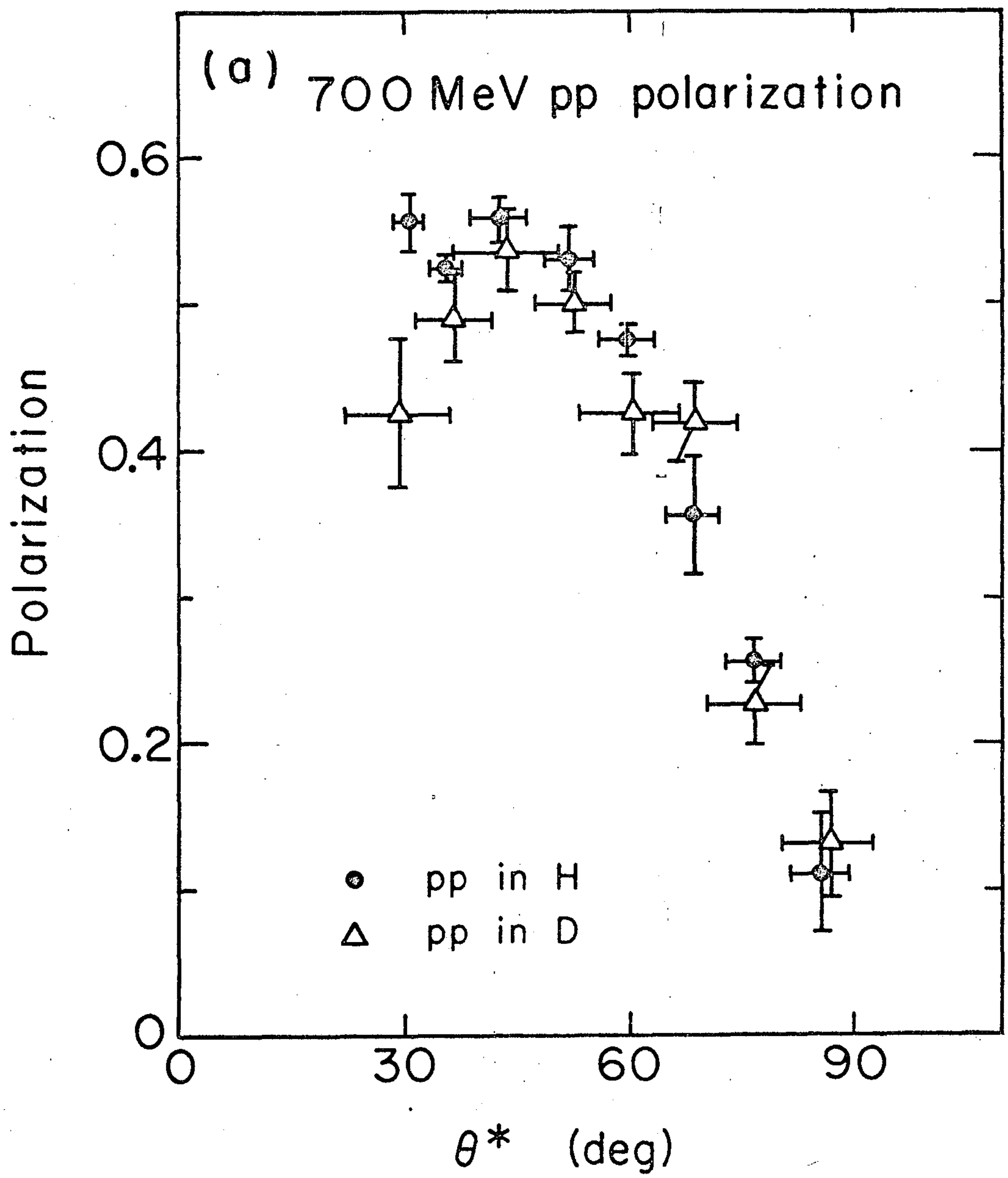

MUB-9503

Fig. 8(a)

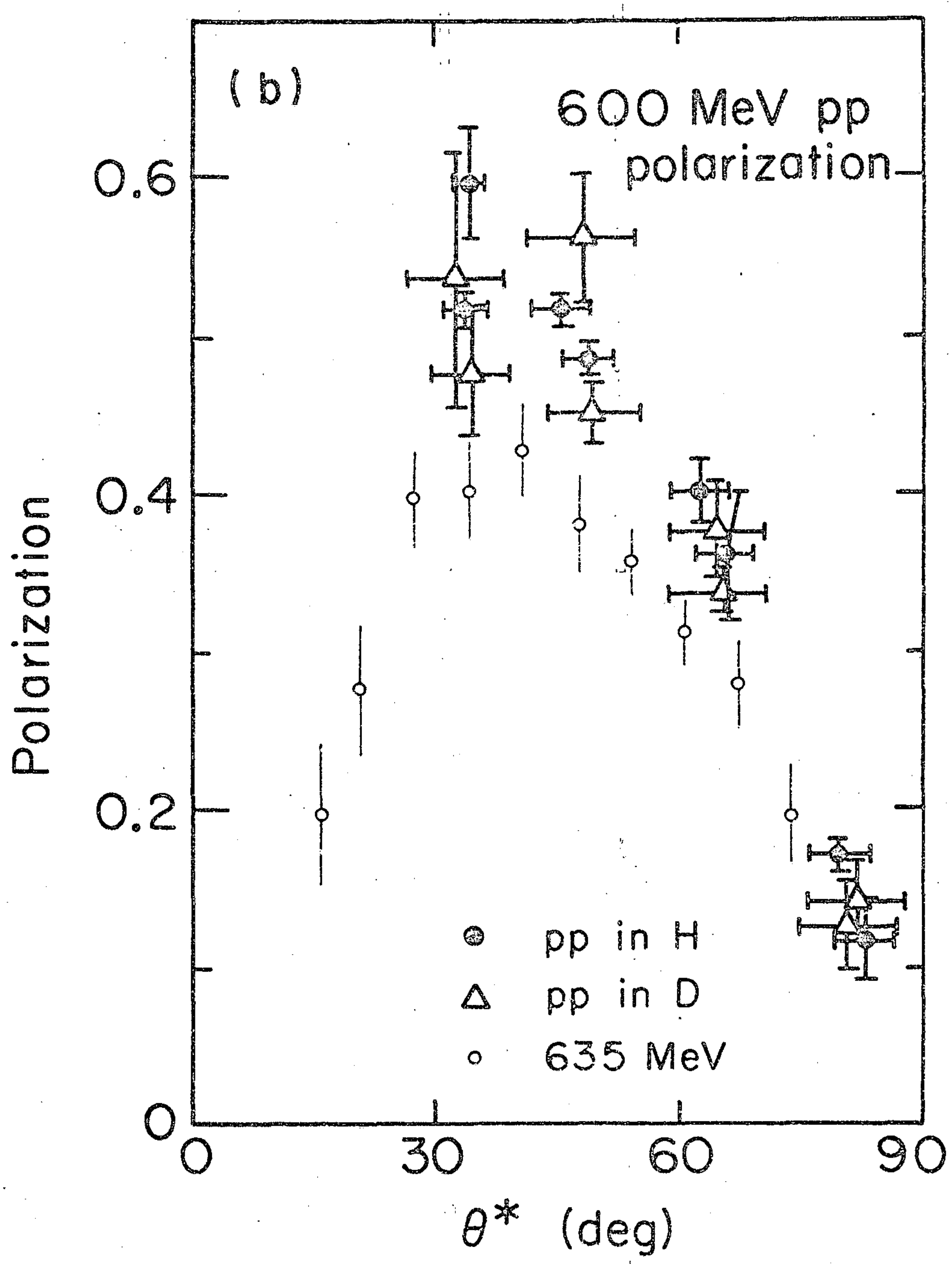

MU-36247

Fig. 8(b)

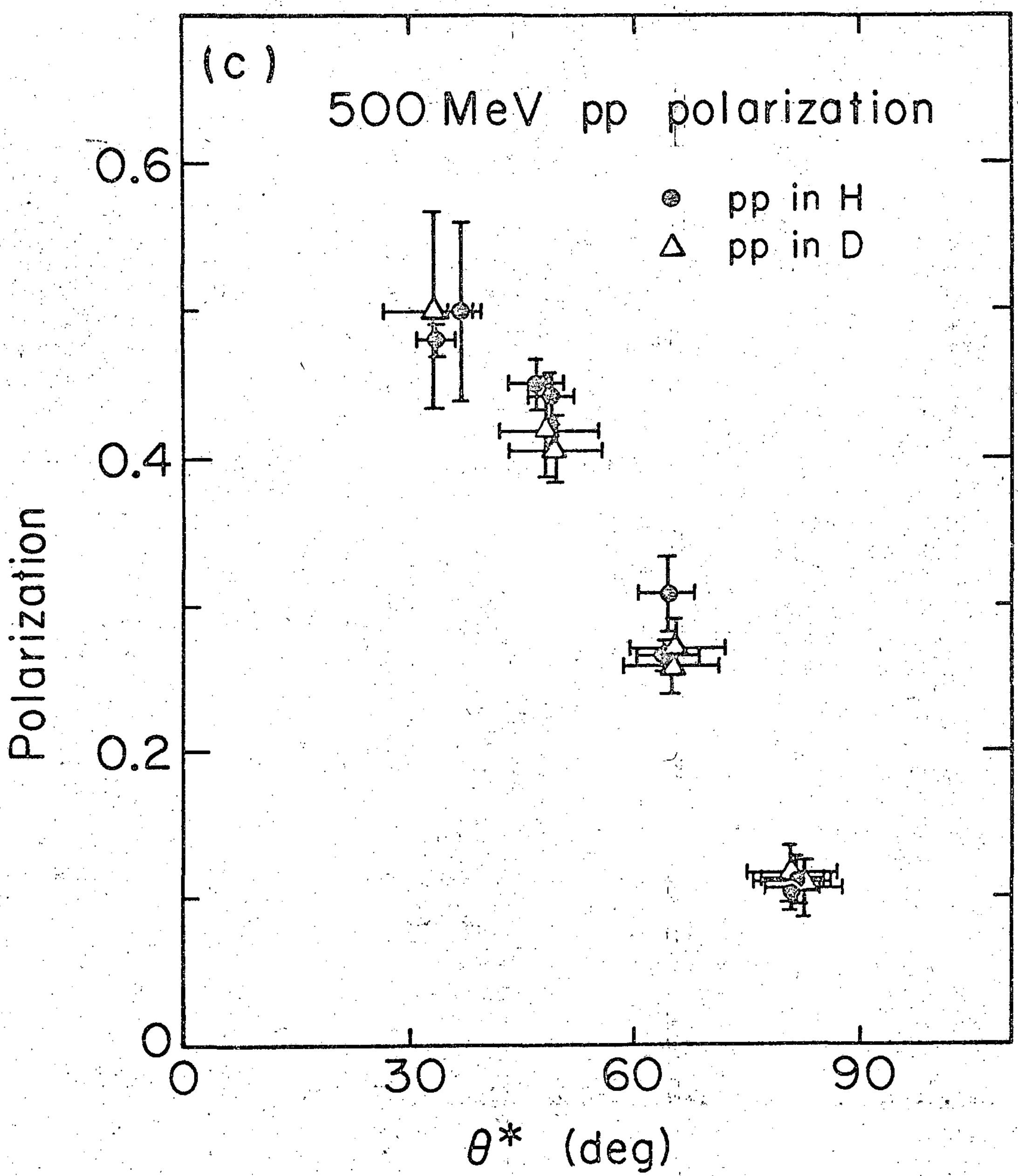

MUB-9502

Fig. 8(c)

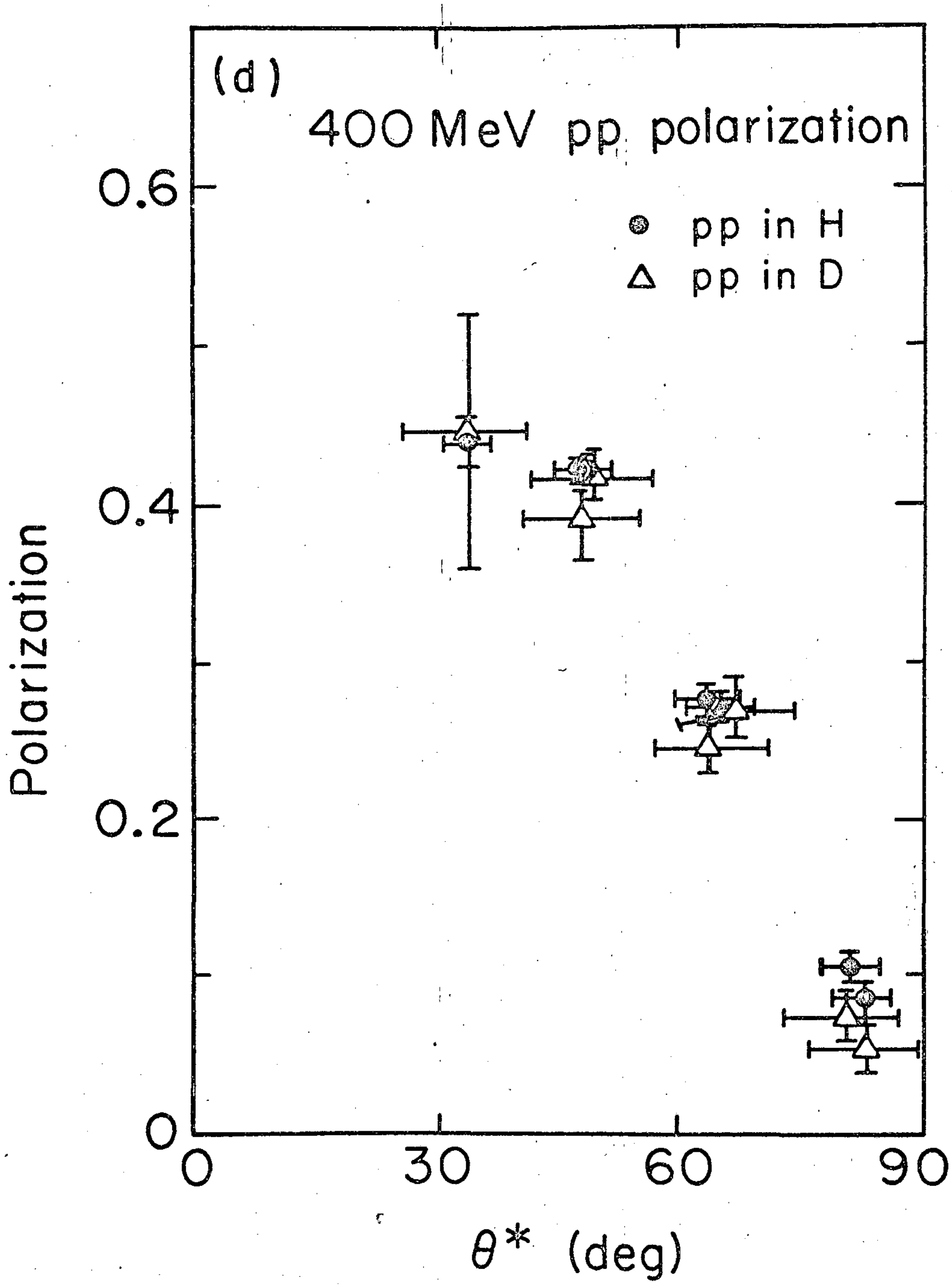

MU-36258

Fig. 8(d)

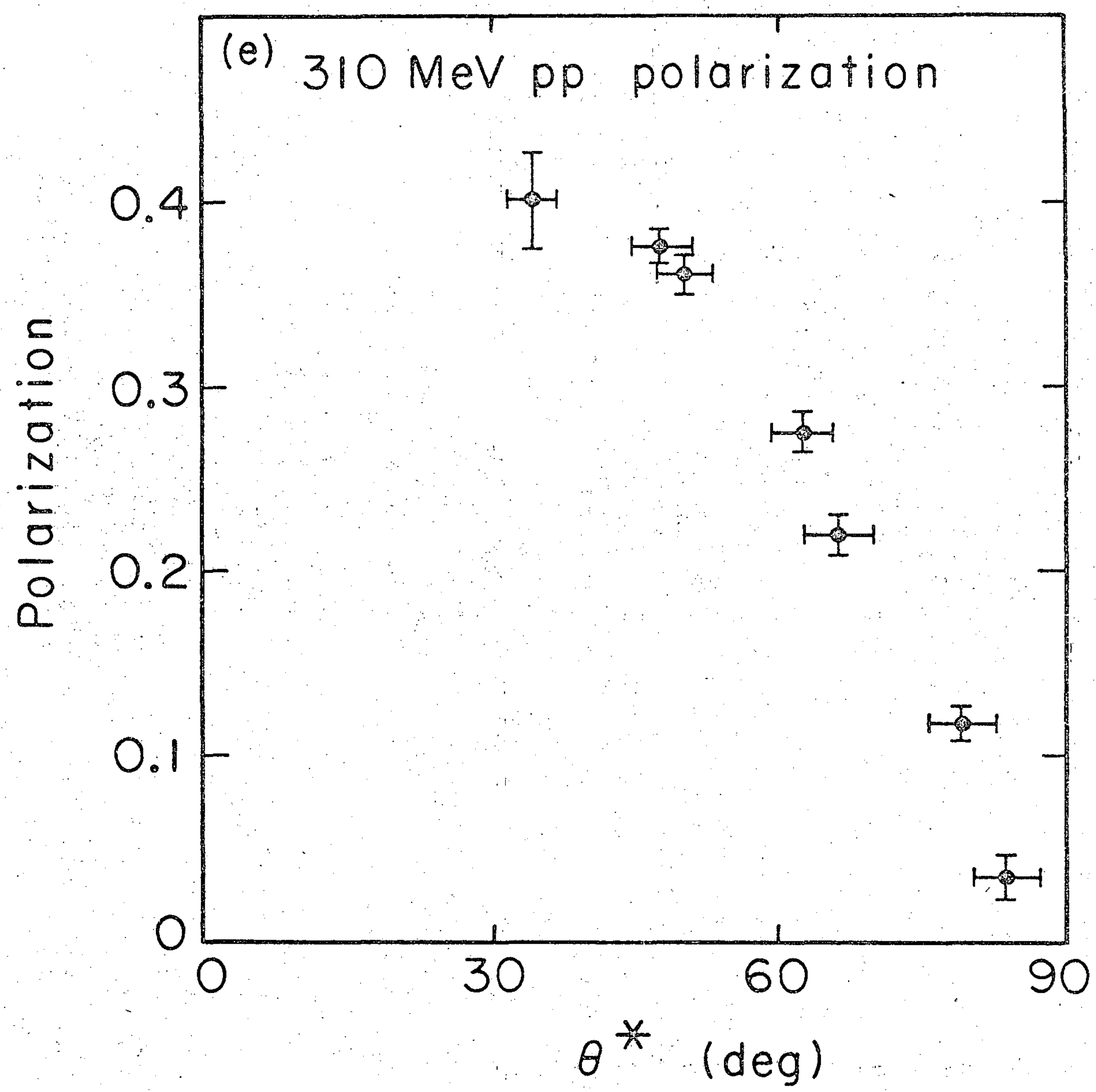

MU-36242

Fig. 8(e)

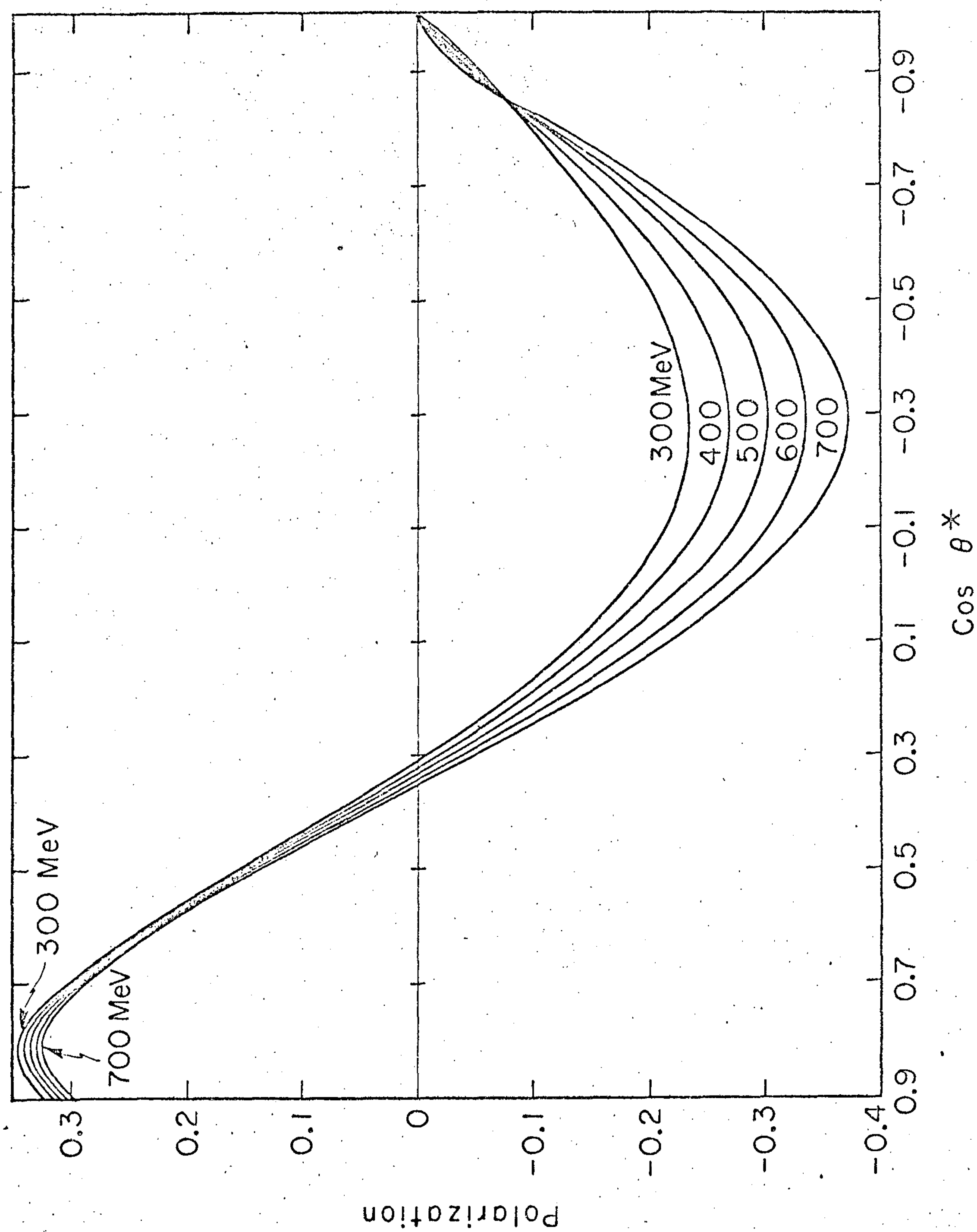

Fig. 9

MU-36244

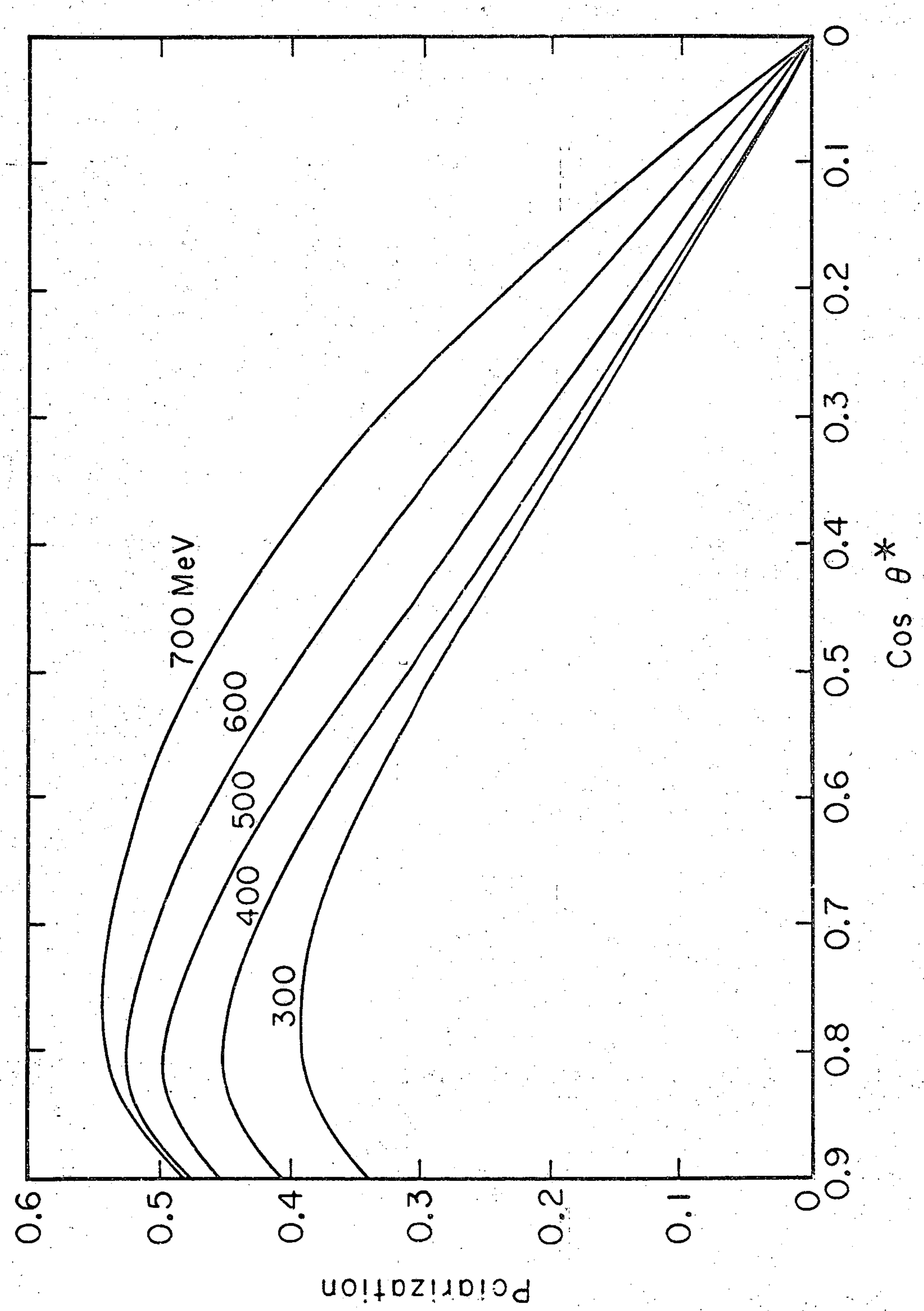

MU-36245

Fig. 10

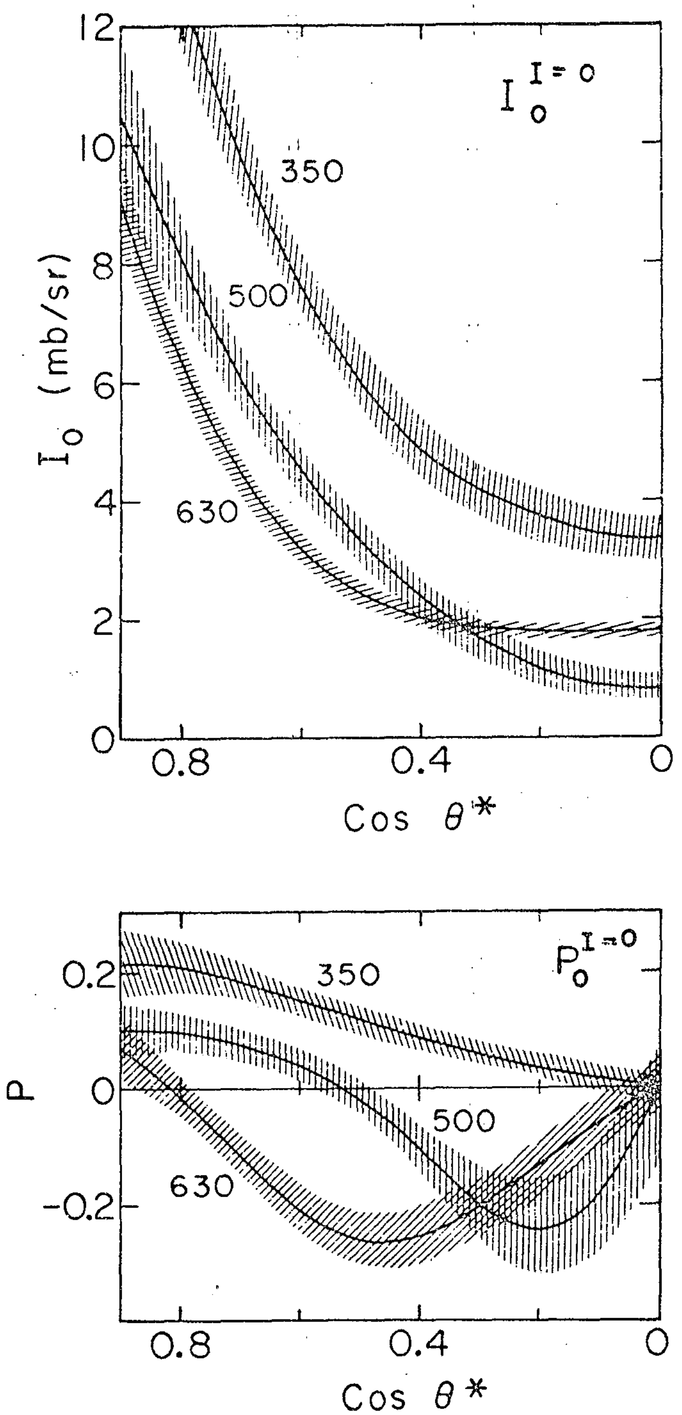

XBL671-402

Fig. 11